# Feasibility of Battery-Powered Propulsion Systems for All-Electric Short-Haul Commuter Aircraft

Markus Aasen Anker [1], Christian Hartmann [1], and Jonas Kristiansen Nøland [2]

[1]Affiliation not available
[2]Norwegian University of Science and Technology (NTNU)

July 10, 2023

# Feasibility of Battery-Powered Propulsion Systems for All-Electric Short-Haul Commuter Aircraft

Markus Aasen Anker, Christian Hartmann, *Member, IEEE*, and Jonas Kristiansen Nøland, *Senior Member, IEEE*

***Abstract*—All-electric battery-powered aircraft have, over the last couple of years, had a clear path toward commercialization by the end of this decade. However, the development of smaller all-electric commuter aircraft has recently stagnated due to inherent technical limitations. To gain deeper insights into these challenges, this paper provides a detailed powertrain analysis of 9- and 19-seat all-electric commuter aircraft. Real-world mission profile data, obtained from 1500 flights in the Norwegian short-haul route network (i.e., flights shorter than 200 nautical miles), are used as inputs. Regression analysis reveals that the cruising power needed is only about $43\,\%$ of the power needed for takeoff and climb. Our work presents a comprehensive component-level weight distribution analysis of the all-electric powertrains investigated, and the required weight is shown to exceed the manufacturers' reported maximum takeoff weight (MTOW) of the two reference aircraft studied. However, small improvements in component performances could make electrification of the short-haul route network feasible, which is highlighted in a sensitivity study of the most critical electrical components. Additionally, our study highlights that the shortest missions are actually dimensioned by power rating rather than energy storage, adding an extra constraint on battery sizing for the shortest trips.**

***Index Terms*—Battery-electric aircraft, commuter aircraft, short-haul route network, all-electric propulsion, thermal management system, mission profile modeling, motion modeling.**

## NOMENCLATURE

| | |
|---|---|
| $\dot{Q}_{bat}$ | Battery's heat losses, [kW] |
| $\dot{Q}_{bcb}$ | Battery DC circuit breaker heat losses, [kW] |
| $\dot{Q}_{cab1}$ | Primary cable heat losses, [kW] |
| $\dot{Q}_{cab2}$ | Auxiliary cable heat losses, [kW] |
| $\dot{Q}_{cb1}$ | Primary AC circuit breaker heat losses, [kW] |
| $\dot{Q}_{cb2}$ | Auxiliary AC circuit breaker heat losses, [kW] |
| $\dot{Q}_{conv}$ | DC/DC converter heat losses, [kW] |
| $\dot{Q}_{gear}$ | Gear's heat losses, [kW] |
| $\dot{Q}_{inv1}$ | Primary DC/AC inverter heat losses, [kW] |
| $\dot{Q}_{inv2}$ | Auxiliary DC/AC inverter heat losses, [kW] |
| $\dot{Q}_{mot}$ | Motor's heat losses, [kW] |
| $\dot{Q}_{tot}$ | Total heat losses, [kW] |
| $\eta_{bat}$ | Battery efficiency, [%] |
| $\eta_{cab}$ | Cable efficiency, [%] |
| $\eta_{cb1}$ | Unidirectional DC circuit breaker efficiency, [%] |
| $\eta_{cb2}$ | Bidirectional AC circuit breaker efficiency, [%] |
| $\eta_{conv}$ | DC/DC converter efficiency, [%] |
| $\eta_{gear}$ | Gear efficiency, [%] |
| $\eta_{inv}$ | DC/AC inverter efficiency, [%] |
| $\eta_{mot}$ | Motor efficiency, [%] |
| $\eta_{tot}$ | System-level overall efficiency, [%] |
| PAX | Number of passengers |
| $\mu$ | Friction coefficient |
| $\rho$ | Air's mass density, [kg/m$^3$] |
| $a$ | Aircraft acceleration, [m/s$^2$] |
| $C_D$ | Aerodynamic drag coefficient |
| $C_L$ | Aerodynamic lift coefficient |
| $D$ | Aircraft's drag force, [N] |
| $E_{bat}$ | Battery energy content, [kWh] |
| $e_{bat}$ | Battery's specific energy, [Wh/kg] or [kWh/kg] |
| $E_{tot}$ | Total energy use during flight, [kWh] |
| $F$ | Aircraft's thrust force, [N] |
| $g$ | Gravitational acceleration, [m/s$^2$] |
| $h_{btms}$ | BTMS power per extracted heat loss, [kW/kW] |
| $H_{cruise}$ | Aircraft's cruising height, [m] or [km] |
| $h_{ptms}$ | PTMS power per extracted heat loss, [kW/kW] |
| $i'_{cab}$ | Specific current of distribution grid, [a/kg/m] |
| $K_a$ | Aircraft aerodynamic performance constant, [kg/m] |
| $k_{bat}$ | Battery's utilization factor |
| $k_{gear}$ | Gear constant |
| $L$ | Aircraft's lift force, [N] |
| $L/D$ | Aerodynamic lift-to-drag ratio |
| $l_{cab1}$ | Length of the primary cable for the EPS, [m] |
| $l_{cab2}$ | Length of the auxiliary cable for the TMS, [m] |
| $m_0$ | Aircraft empty weight, [kg] |
| $m_f$ | Aircraft fuel weight, [kg] |
| $m_{bat}$ | Battery weight, [kg] |
| $m_{bcb}$ | Battery DC circuit breaker weight, [kg] |
| $m_{btms}$ | BTMS weight, [kg] |
| $m_{cab1}$ | Primary cable weight, [kg] |
| $m_{cab2}$ | Auxiliary cable weight, [kg] |
| $m_{cb1}$ | Primary AC circuit breaker weight, [kg] |
| $m_{cb2}$ | Auxiliary AC circuit breaker weight, [kg] |
| $m_{conv}$ | DC/DC converter weight, [kg] |
| $m_{gear}$ | Gear weight, [kg] |
| $m_{inv1}$ | Primary DC/AC inverter weight, [kg] |
| $m_{inv2}$ | Auxiliary DC/AC converter weight, [kg] |
| $m_{mot}$ | Motor weight, [kg] |
| $m_{pl}$ | Aircraft payload weight, [kg] |
| $m_{ptms}$ | PTMS weight, [kg] |
| $m_{tot}$ | Total aircraft weight, [kg] |
| $p_{bat}$ | Battery's specific power, [kW/kg] |
| $P_{bcb}$ | Battery DC circuit breaker power output, [kW] |
| $P_{btms}$ | BTMS power consumption, [kW] |
| $p_{btms}$ | Heat loss extracted per BTMS mass, [kW/kg] |
| $P_{cab1}$ | Primary cable power output, [kW] |
| $P_{cab2}$ | Auxiliary cable power output, [kW] |
| $P_{cb1}$ | Primary AC circuit breaker power output, [kW] |
| $p_{cb1}$ | Unidirect. DC circuit breaker spec. power, [W/kg] |
| $P_{cb2}$ | Auxiliary AC circuit breaker power output, [kW] |
| $p_{cb2}$ | Bidirect. AC circuit breaker specific power, [W/kg] |
| $P_{climb}$ | Climbing power output, [kW] |
| $P_{conv}$ | DC/DC converter power output, [kW] |

| | |
|---|---|
| $p_{conv}$ | DC/DC converter's specific power, [kW/kg] |
| $P_{cruise}$ | Cruising power output, [kW] |
| $P_{descent}$ | Descent power output, [kW] |
| $P_{gear}$ | Gear power output, [kW] |
| $P_{inv1}$ | Primary DC/AC inverter power output, [kW] |
| $P_{inv2}$ | Auxiliary DC/AC inverter power output, [kW] |
| $p_{inv}$ | DC/AC inverter's specific power, [kW/kg] |
| $P_{motor}$ | Motor power output, [kW] |
| $p_{mot}$ | Motor's specific power, [kW/kg] |
| $P_{prop}$ | Propulsion power output, [kW] |
| $P_{ptms}$ | PTMS power consumption, [kW] |
| $p_{ptms}$ | Heat loss extracted per PTMS mass, [kW/kg] |
| $P_{takeoff}$ | Takeoff power output, [kW] |
| $P_{thrust}$ | Aerodynamic thrust power, [kW] |
| $p_{tot}$ | System-level overall power density, [kW/kg] |
| $R$ | Aircraft's travel range, [m] or [km] |
| $s$ | Flight distance traveled, [m] or [km] |
| $t_0$ | Takeoff time, [s] or [min] |
| $t_1$ | Top-of-climb time, [s] or [min] |
| $t_2$ | Top-of-descent time, [s] or [min] |
| $t_3$ | Landing time, [s] or [min] |
| $T_{climb}$ | Duration of the flight's climbing phase, [s] or [min] |
| $T_{cruise}$ | Duration of the flight's cruising phase, [s] or [min] |
| $T_{descent}$ | Duration of the flight's descent phase, [s] or [min] |
| $v$ | Aircraft instantaneous velocity, [m/s] or [km/h] |
| $v_\infty$ | Aircraft cruising velocity, [m/s] or [km/h] |
| $v_{takeoff}$ | Aircraft takeoff velocity, [m/s] or [km/h] |
| $W$ | Aircraft's weight force, [N] |
| $\Delta T_{res}$ | Aircraft energy reserve time, [s] or [min] |
| $\theta$ | Aircraft climb angle, [°] or [rad] |
| $S$ | Projected wing surface area [$m^2$] |
| $u_{dc}$ | Voltage level of DC distribution, [V] or [kV] |

## I. Introduction

THE aviation industry has been growing steadily and its emissions currently contribute to $2.7\,\%$ of global $CO_2$ emissions and $5\,\%$ of Anthropocene temperature change [1]. However, with demand projected to increase by $4.3\,\%$ annually [2], the industry may contribute with up to $20\,\%$ of global $CO_2$ emissions by 2050. To mitigate the increased $CO_2$ emissions, the aviation sector aims to achieve net zero emissions by 2050 through technological advancements and a transition to sustainable energy sources, including aircraft electrification. Switching to all-electric aircraft has several benefits beyond emission reductions. Electric powertrains are more energy-efficient than conventional jet engines, which have significant energy losses. With electric drivetrains, efficiency targets exceed $90\,\%$ [3]. Electric aircraft also produce fewer harmful non-$CO_2$ emissions like $NO_x$ and $CO$ and improve air quality around airports [4]. Electric powertrains have fewer parts, increasing reliability, and they reduce noise pollution experienced by people living near airports [5]. Lower noise could lead to the expansion of near-city urban airports, which are currently restricted by noise requirements [6]. Additionally, electric aircraft could offer new design optimization opportunities, lower operation costs, and increased mobility [7].

While electric aviation has obvious advantages, it is still in its infancy. Nevertheless, one all-electric aircraft, the Velis Electro produced by Pipistrel, has been fully certified for operation by the European Union Aviation Safety Agency (EASA) as of June 2020. However, the challenges facing the transformation toward electric aircraft are significant, with limited scalability of energy storage as the primary barrier. Conventional aircraft use energy-dense jet fuels of $11.9\,\mathrm{kWh/kg}$, while modern batteries are inherently less energy-dense, with the most promising compositions reaching $0.25\,\mathrm{kWh/kg}$ at the pack-level. As a result, all-electric aircraft are inherently heavy, posing a significant disadvantage for scaling up the technology. Electric aviation will initially facilitate short-distance flights due to the significant weight of energy storage. In this context, the Norwegian short-haul route network has been identified as one of the initial deployment arenas with the ambitious Norwegian target of electrifying the domestic airline industry by 2040.

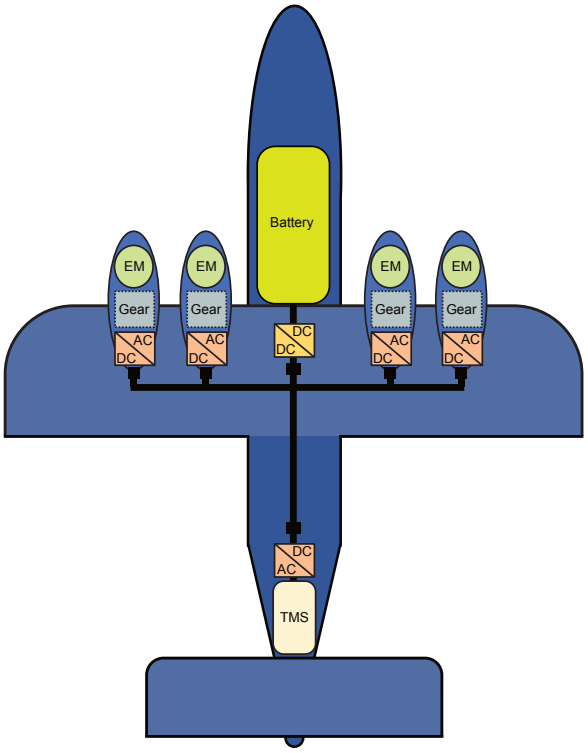


Fig. 1. Generic electric propulsion system (EPS) onboard a four-motor commuter aircraft, including battery storage, DC/DC converter, DC/AC inverters, gears, electric motors (EMs), and thermal management system (TMS).

To address the need for electric aircraft solutions, several start-up companies have in recent years announced launch dates for their all-electric aircraft designs. These designs range from complete retrofits, where the conventional propulsion unit of an existing design is replaced by an electrical one, to new designs utilizing the design freedom offered by electrification. Table I summarizes some key companies developing all-electric aircraft. Of them, Zeroavia and Eviation are the only ones that have performed their maiden flights. Recently, Heart, NASA, and Tecnam announced postponed launch dates.

There are currently a myriad of challenges to be addressed to mature electric aviation technology. Among them are the need to develop lightweight, fault-tolerant, and reliable electri-

TABLE I
OVERVIEW OF ORIGINALLY ANNOUNCED ALL-ELECTRIC COMMUTER AND REGIONAL AIRCRAFT

| Company | Model | Technology | Preliminary launch | Capacity | Source |
|---|---|---|---|---|---|
| NASA | X-57 Maxwell | Battery-electric | n/a[1] | 2 PAX | nasa.gov |
| Elfly Group | X10 | Battery-electric | 2029 | 9 PAX | el-fly.no |
| Eviation | Alice | Battery-electric | 2027 | 9 PAX | eviation.com |
| Tecnam | P-Volt | Battery-electric | 2026[2] | 9 PAX | tecnam.com |
| Bye Aerospace | eFlyer 800 | Battery-electric | 2027 | 12 PAX | byeaerospace.com |
| Heart Aerospace | ES-19 | Battery-electric | 2026[3] | 19 PAX | heartaerospace.com |
| Heart Aerospace | ES-30 | Hybrid-electric | 2028 | 30 PAX | heartaerospace.com |
| ZeroAvia | ZA600 | Hydrogen-electric | 2025 | 10-20 PAX | zeroavia.com |
| Wright Electric | Spirit | Hydrogen-electric | 2026 | 100 PAX | weflywright.com |

[1] The program was discontinued by NASA, [2] Temporarily paused due to immature battery technology,
[3] Heart Aerospace dropped their ES-19 project to instead focus on the larger 30-passenger hybrid-electric ES-30.

cal components [8]. To understand these issues, comprehensive technology status reviews have been presented [9]–[12]. Based on existing and projected electric aircraft performances, power and energy requirements have been established to evaluate the scalability [13]–[15]. However, future projections for technology development may be overly optimistic, as they overlook the need for disruptive technological advancements to achieve the projected performance targets [16]–[18]. Moreover, transitioning from a successful prototype to a commercially available product requires significant time and effort [19]. Other challenges include redundancy requirements for electrical components and the allocation of sufficient energy reserves to comply with aircraft certification regulations.

This paper aims to evaluate the feasibility of an all-electric commuter aircraft powertrain and highlight technological and regulatory challenges that may hinder its adoption. Our focus is on short-haul routes under 200 nautical miles with less than 19 passengers, aligning with the EASA CS-23 aircraft certification standard. In contrast, existing studies, such as Gnadt *et. al.* (2019) [20] and Marciello *et. al.* (2023) [21], investigate the design aspects of electric aircraft for regional flights longer than 400 nautical miles and carrying 50 to 180 passengers. The present paper is concerned with 9- and 19-seat commuter aircraft powertrains and provides a comprehensive weight analysis at the component level. Our power and energy analysis encompasses all flight phases, including takeoff, climb, cruise, and descent, backed up by statistical insights gleaned from 1500 flights on the Norwegian short-haul route network. It is worth noting that prior preliminary work focused solely on the cruising phase [22]. Nevertheless, another study by Bærheim *et. al.* (2023) analyzed the power and energy requirements for complete mission profiles [23], although only focusing on the battery sizing and modeling while overlooking all other components in the aircraft powertrain. This paper comprehensively addresses all components of the electric propulsion system (EPS) and gives due consideration to the often-neglected thermal management system (TMS), a critical factor in the overall weight of the powertrain.

Fig. 1 illustrates the principal elements of our studied four-propeller powertrain, which include electric motors, inverters, converters, TMS, and battery management system (BMS). From the generalised powertrain, our work derives a detailed-level weight-sizing model for analysing commuter aircraft powertrains, with a breakdown of the mass contribution of each electrical component. This component-level analysis enables a better understanding of the most critical issues for electrifying commuter aircraft. Additionally, the study shows the impact of various regulations, including requirements on reserve energy and redundancy, on the aircraft's weight. The work also contains a sensitivity analysis where central performance parameters are allowed to vary. This helps identify what impact various technological improvements have on the overall aircraft performance. This will inform the feasibility of all-electric commuter flights by the end of this decade and help to target the areas that may hinder their realization.

Our work presents statistical analysis of short-haul commuter flights based on data collected from 1500 flights covering varying distances, where the mission profiles include time regressions based on flight distance. A complete overview of weekly flights on the network is provided, taking into account factors such as airport infrastructure and flight time. The study is motivated by Jux *et. al.* (2018) [24], which used a similar methodology to establish a standard mission profile focusing on regional flights lasting approximately an hour. In contrast, this paper analyses substantially shorter routes, which has been, until now, overlooked in the research literature.

The rest of the paper is structured as follows. Section II presents the chosen case studies, both selected routes and representative commuter aircraft. The following Section III describes the Norwegian short-haul route network and collects data from 1500 flights that are further processed to identify the most important patterns in the mission profile. A generalized power and time profile for commuter flights is established to inform further analysis. Then, the aircraft powertrain modeling is described in Section IV, including basic aerodynamics, power and energy requirements, powertrain sizing, and energy storage dimensioning. Finally, Section V presents the main results of the paper's chosen case studies, including sensitivity analysis, before concluding the paper in Section VI.

## II. CHOSEN CASE STUDIES

This paper's selected short-haul routes and representative commuter aircraft are depicted in Fig. 2. The flights analyzed fall within the shorter range of the Norwegian short-haul route network, with the longest distance being $211\,\mathrm{km}$ from Tromsø to Hammerfest (Route 4). However, shorter routes are also considered to assess the potential for early-stage aircraft electrification. Table II describes the key metrics of the four

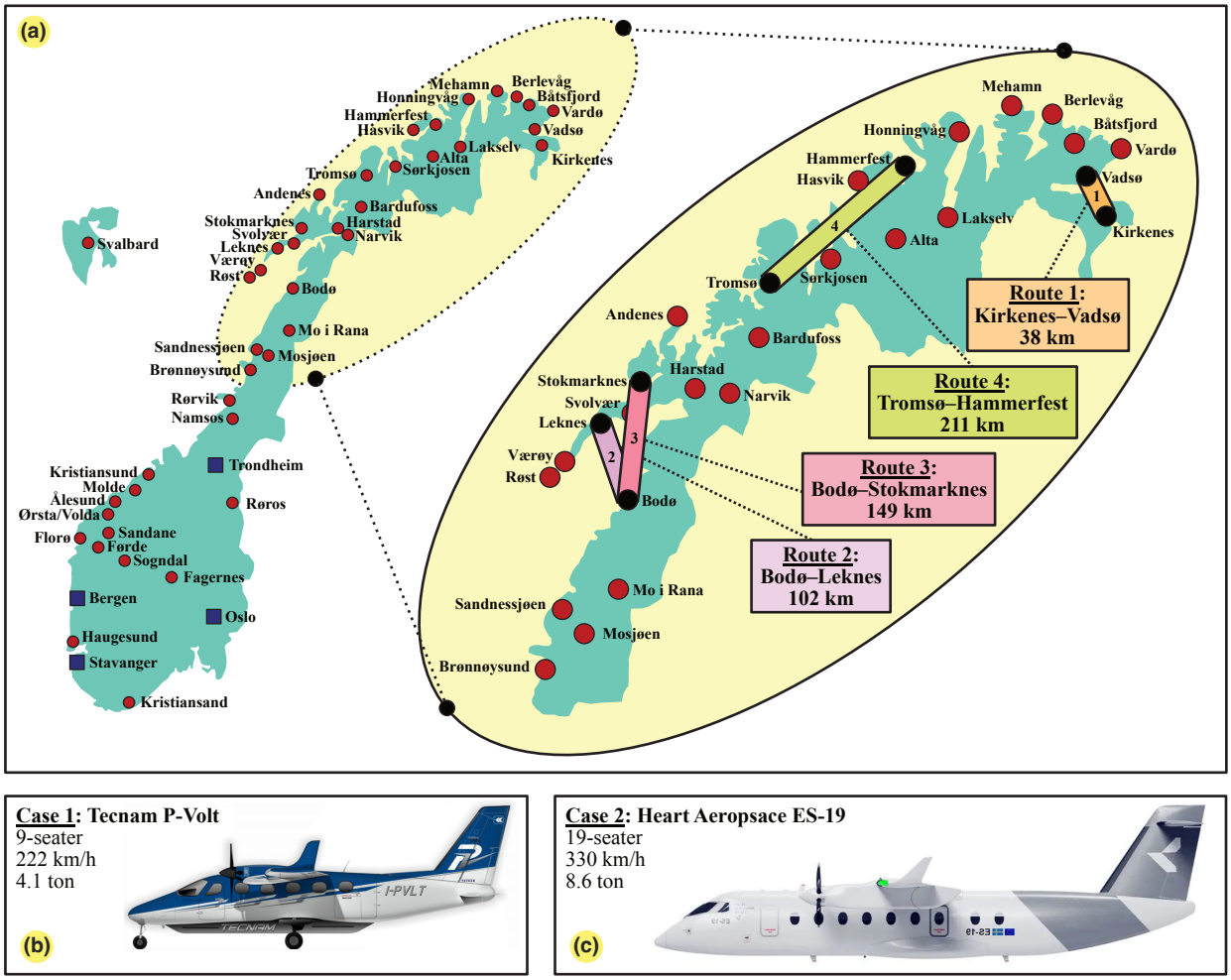


Fig. 2. An overview of the chosen flight distances in the Norwegian short-haul regional network and the studied commuter aircraft. **(a):** Routes 1–4. **(b):** Case 1 aircraft. **(c):** Case 2 aircraft.

TABLE II
SHORT-HAUL COMMUTER ROUTES INCLUDED IN THE CASE STUDY

| Route number | Airports | Flight distance ($s$) | Avg. flight time ($\Delta t$) | Weekly flights |
|---|---|---|---|---|
| Route 1 | Kirkenes-Vadsø | 38 km | 11 min | 34 |
| Route 2 | Bodø-Leknes | 103 km | 25 min | 72 |
| Route 3 | Bodø-Stokmarknes | 149 km | 35 min | 59 |
| Route 4 | Tromsø-Hammerfest | 211 km | 45 min | 92 |

routes examined, and their relevance for electrification can be understood from their relatively high flight frequency.

The representative aircraft selected for this study are Tecnam's P-Volt and Heart Aerospace's ES-19, which were turboprop aircraft capable of STOL operation targeting the short-haul market. However, at the current stage, Tecnam's P-Volt has been paused while waiting for the evolution of battery technology (claiming that they had battery storage capacity of just $0.17\,\mathrm{kWh/kg}$) and Heart Aerospace has announced its decision to switch from its 19-seat ES-19 electric commuter aircraft to a larger 30-seat version (ES-30). Despite these developments, the paper will use these aircraft as a reference as it could give insight into the decisions by Tecnam and Heart Aerospace. Therefore, our study focus on real-world use cases that have been recently hindered due to technical obstacles.

### A. Case 1: Tecnam P-Volt (9-seater)

The P-Volt, a collaboration between Tecnam and Rolls Royce, is based on the P2012 Traveller and gains significance due to Widerøe's participation as a project partner. Widerøe plans to purchase and operate the aircraft on Norway's short-haul routes. With a capacity for nine passengers and two pilots, the P-Volt is expected to offer a range of $157\,\mathrm{km}$, making it suitable for three out of the four routes in our case study. Table III presents a comparison of the P-Volt's specifications with similar aircraft of its size. While the P-Volt has the same outer dimensions as its conventional engine counterpart, the P2012 Traveller, its maximum takeoff weight (MTOW) exceeds that of the P2012, likely due to the added battery weight. Nonetheless, the P-Volt remains the lightest aircraft among the models listed in the table.

The Eviation Alice, another electric aircraft in development, boasts unique design features compared to the P-Volt. It claims to offer an impressive range of up to $450\,\mathrm{km}$ and twice the cruise speed. However, its increased range may contribute to its higher weight compared to the P-Volt. Furthermore, the

TABLE III
SPECIFICATIONS OF THREE DIFFERENT 9-SEATER COMMUTER AIRCRAFT COMPARED TO SELECTED CASE 1 AIRCRAFT

| Symbol | Alternatives | | | Case 1: |
|---|---|---|---|---|
| | Pilatus PC-12 | Tecnam P2012 Traveller | Eviation Alice | Tecnam P-Volt |
| | Regular | Regular | All-electric | All-electric |
| $w$ | 16.28 m | 14.00 m | 19.20 m | 14.00 m |
| $l$ | 14.40 m | 11.80 m | 17.40 m | 11.80 m |
| $m_{max}$ | 4740 kg | 3680 kg | 8346 kg | 4086 kg |
| $m_0$ | 2810 kg | 2286 kg | n/a | 2177 kg |
| $P_{prop}$ | 2×445 kW | 2×275 kW | 2×700 kW | 2×320 kW |
| $v_{cruise}$ | n/a | 320 km/h | 464 km/h | 222 km/h |
| $v_{max}$ | 537 km/h | 359 km/h | 481 km/h | 333 km/h |

Sources: pilatus-aircraft.com, eviation.com, & tecnam.com

TABLE IV
SPECIFICATIONS OF THREE DIFFERENT 19-SEATER COMMUTER AIRCRAFT COMPARED TO SELECTED CASE 2 AIRCRAFT

| Symbol | Alternatives | | | Case 2: |
|---|---|---|---|---|
| | Beech King 1900D | Jetstream 31 | Fairchild D228 | Heart Aerospace ES-19 |
| | Regular | Regular | Regular | All-electric |
| $w$ | 15.85 m | 17.67 m | 16.97 m | 23.00 m |
| $l$ | 14.37 m | 17.63 m | 16.56 m | 14.50 m |
| $m_{max}$ | 6950 kg | 7688 kg | 6400 kg | 8600 kg |
| $m_0$ | 4730 kg | 4360 kg | 3740 kg | 3600 kg |
| $P_{prop}$ | 2×380 kW | 2×477 kW | 2×265 kW | 4×400 kW |
| $v_{cruise}$ | 482 km/h | 426 km/h | 350 km/h | 330 km/h |
| $v_{max}$ | 519 km/h | 487 km/h | n/a | n/a |

Sources: globalair.com, skybrary.aero, & heartaerospace.com

Alice's higher weight and speed might necessitate a higher installed power, potentially further impacting its weight.

### B. Case 2: Heart Aerospace ES-19 (19-seater)

The Swedish start-up Heart Aerospace's ES-19, a 19-seater aircraft, demonstrated a subscale version showcasing its four-motor design, proven for reliability. It claims a 400 km range, surpassing the P-Volt, suitable for most Norwegian short-haul routes. Its four motors provide propulsion redundancy and enhance STOL capabilities, essential given its high weight.

TABLE V
OVERVIEW OF WIDERØE'S SHORT-HAUL FLEET

| Aircraft type | Quantity | Capacity | Max cruise speed |
|---|---|---|---|
| E190-E2 | 3 | 110 PAX | 890 km/h |
| DASH-8 Q400 | 10 | 78 PAX | 667 km/h |
| DASH-8 300 | 4 | 50 PAX | 501 km/h |
| DASH-8 100/Q200 | 26 | 39 PAX | 482 km/h, 518 km/h |

Source: airfleets.net/flottecie/wideroe.htm

The ES-19's wide wingspan, relative to its length, is likely to accommodate the four propellers.

Table IV compares the ES-19 to other 19-seater aircraft, showing its lower empty weight but higher MTOW and lower cruise speed, mirroring trends seen with the P-Volt.

## III. ROUTE NETWORK AND FLIGHT PROFILE ANALYSIS

Norway's short-haul route network, mainly in its northern and western regions, is a promising testbed for electric aviation. Built in the 1960s and 70s to enhance mobility in rural areas, these airports are crucial due to the mountainous terrain, fjords, and islands that make air travel the most viable mode of transportation in this region.

Fig. 3 presents data on weekly flights in Norway's short-haul route network, highlighting that most flights cover 100-150 km, which is the main focus hereafter. Widerøe, the main operator in this segment, has its fleet detailed in Table V.

### A. Collection of Real-World Flight Data

This study analyzes Norwegian short-haul route network to establish a standardized mission profile using actual flight data, motion equations, and statistical post-processing. We present a power distribution for various flight phases, extending the work of Jux *et al.* (2018) [24] to short-haul distances below 200 nautical miles, using a time regression model based on climb, cruise, and descent durations. The analysis utilized data from Flightradar24, collected from January to April 2022, encompassing 1500 flights, as detailed in Table VI. The Flightradar24 data for our study varied in quality, with

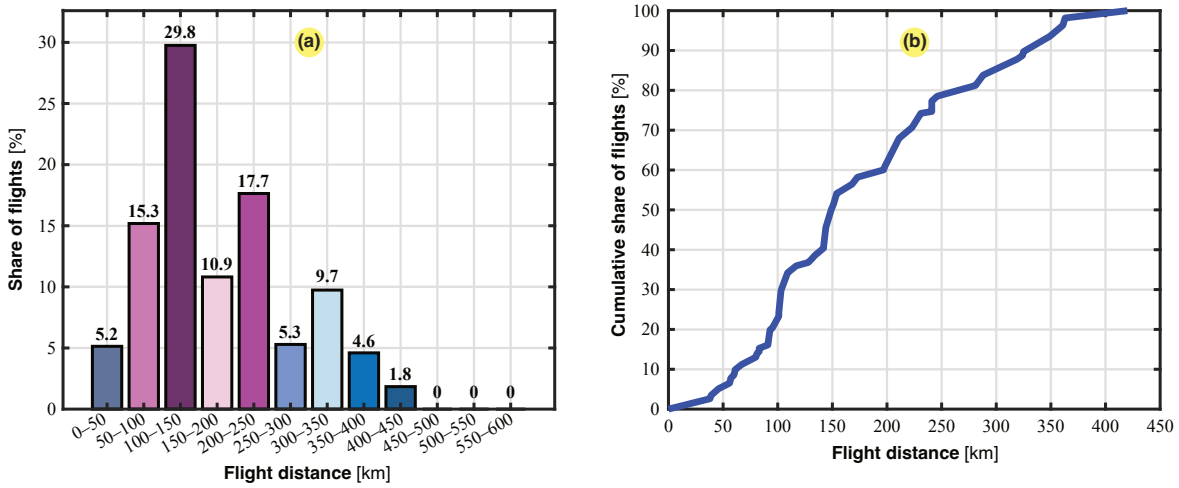


Fig. 3. **(a):** Distribution of flights by travel distance on the Norwegian short-haul network. **(b):** Cumulative distribution of flights covered by flight length.

TABLE VI
FORMAT OF COLLECTED DATA AND EXAMPLE OF A SINGLE STREAM OF VALUES

| Timestamp | UTC | Callsign | Position | Altitude | Speed | Direction |
|---|---|---|---|---|---|---|
| 1651482507 | 2022-05-02T09:08:27Z | WIF932 | "69.676331,18.914303" | 1200 | 107 | 14 |

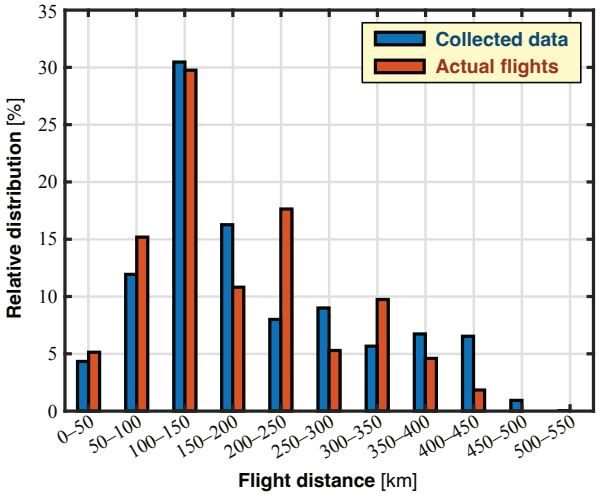


Fig. 4. Comparison of the relative distribution of collected data and the data of planned flights on the short-haul regional network.

some incomplete datasets and inconsistent sampling rates, especially during takeoff, affecting the accuracy of acceleration measurements. To standardize, we required data with frequent sampling during takeoff, ground-level takeoff and landing altitudes, no route diversions, and constant cruising altitudes. Initially, we also sought data with zero initial and final speeds to assess taxiing power and energy needs, but this was challenging to obtain. Our dataset underrepresented certain routes due to insufficient data, leading to some discrepancies, as shown in Fig. 4. This figure also illustrates differences in flight distances, with deviations increasing beyond $150\,\mathrm{km}$ and overrepresentation in the $200$-$250\,\mathrm{km}$ range. Some collected flights included loiters and detours, causing longer than typical distances. Fig. 5 shows a handpicked example of a typical flight's altitude, speed, and power profile, with the highest power demand during takeoff.

### B. Mission Profile Analysis and Post-Processing

The collected flight data is used to create the mission profiles, where a generalized flight profile is developed through regression analysis of the data points.

*1) Takeoff Phase:* The takeoff phase data had notable discrepancies due to low sampling rates, with recorded takeoff times ranging from 1 to 100 seconds. To address this, takeoff time was estimated using the shortest airfield (800 meters) as a reference, appropriate for the short-haul network. The takeoff speed analysis showed an average of approximately 180 km/h, mainly between 170 and $190\,\mathrm{km/h}$, aligning with existing technical data [25]. For power requirements, the study assumed maximum motor output during takeoff, a common approach in aviation research [24], [26], [27], resulting in 32 seconds of full power for this phase.

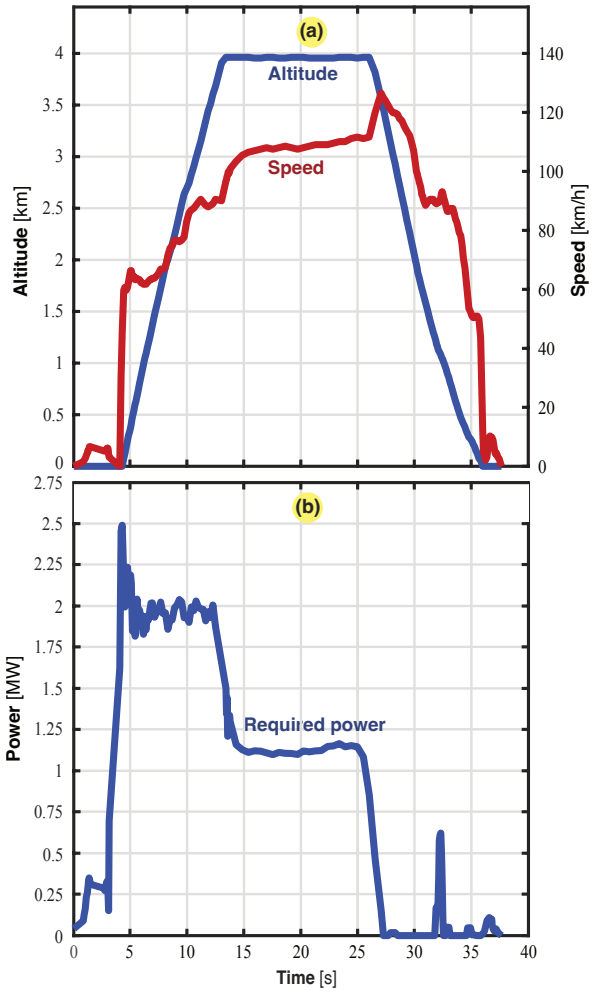


Fig. 5. Example of a mission profile from Tromsø to Hasvik on February 15th, 2022 (Flight WIF7GT). **(a):** Altitude and speed profile. **(b):** Required Dash-8 Q100 propulsion power assuming standard parameters in Table VIII.

*2) Climb Phase:* Figs. 6-(a) and 7-(a) present the collected data for the climb time and the frequency of variation in the normalized power.

*3) Cruising Phase:* Figs. 6-(b) and 7-(b) present the collected cruise time and propulsion power variation data. Cruising heights for short-haul flights are shown in Fig. 6-(c). Standard cruise altitude for regional flights is around $10\,\mathrm{km}$, but it's notably lower for short-haul routes and varies with flight distance. The data shows standardized altitude levels with outliers, particularly in long flights at low altitudes, likely due to extended loiters. The relationship between distance and altitude is linear up to about $300\,\mathrm{km}$, then stabilizes, with the highest flights at approximately $7.6\,\mathrm{km}$, the service ceiling of the Dash-8 100. For aircraft capable of higher ceilings, the cruise altitude could increase. The regression line in the figure illustrates these trends, but it only applies up to $475\,\mathrm{km}$.

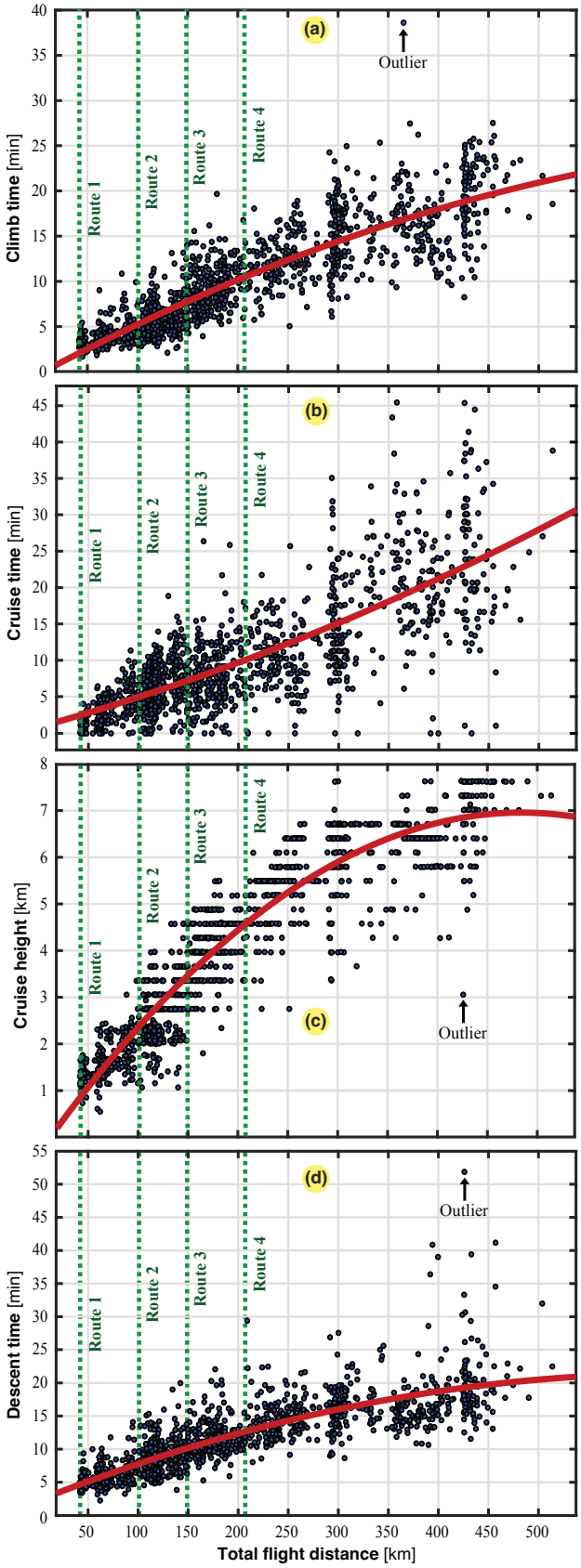


Fig. 6. Regression analysis of 1500 flights. **(a):** Climb time ($T_{climb}$). **(b):** Cruise time ($T_{cruise}$). **(c):** Cruise height ($H_{cruise}$). **(d):** Descent time ($T_{descent}$).

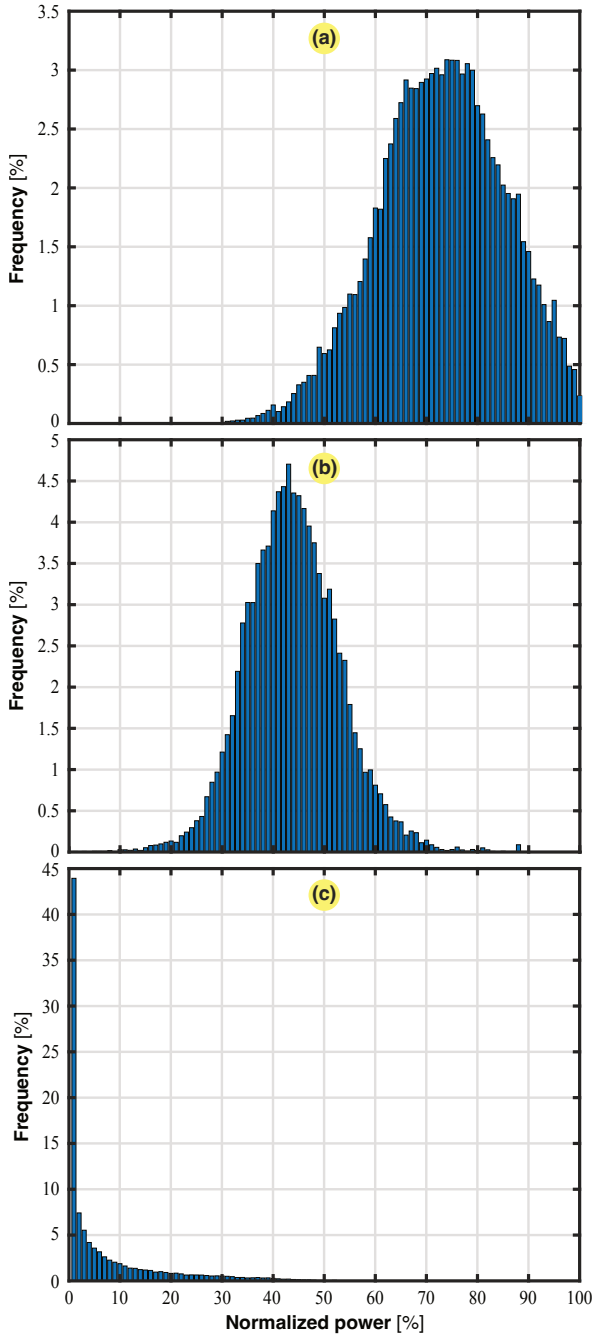


Fig. 7. Frequency occurrence power distribution of 1500 flights. **(a):** Climb power ($P_{climb}$). **(b):** Cruise power ($P_{cruise}$). **(c):** Descent power ($P_{descent}$).

*4) Descent Phase:* Finally, Figs. 6-(c) and 7-(d) show the collected data for the descent time and frequency of variation in the normalized propulsion power during descent.

The mission data is normalized by both flight time and flight distance to establish a normalized profile for the Norwegian short-haul network, which is plotted in Fig. 8. Approximations for the climb, cruise, and descent time as a function of flight distance is listed in Table VII. The cruise height is also included.

To ensure reproducibility, Table VIII provides standard parameters needed to recreate the aircraft power profiles in Fig. 8 using the mission profile data, and the aerodynamic

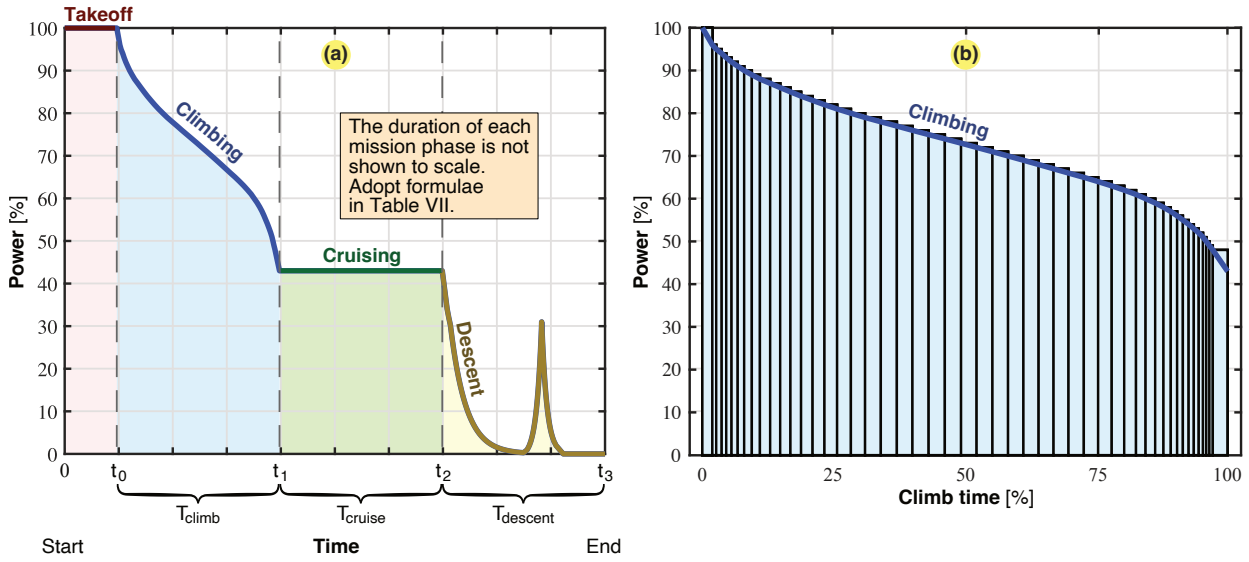


Fig. 8. **(a):** Normalized mission profile used for approximating the collected data under takeoff, climbing, cruising, and descent. **(b):** Normalized climb profile indicating the length of each finite time step derived from the frequency plot.

TABLE VII
CLIMB, CRUISE AND DESCENT TIMES IN SECONDS AND CRUISE HEIGHT IN METERS AS A FUNCTION OF DISTANCE TRAVELED IN KILOMETERS OBTAINED FROM REGRESSION ANALYSIS

| Regression approximation | Data from |
|---|---|
| $T_{climb} \approx -0.002016s^2 + 3.567s - 25.09$ | Fig. 6-(a) |
| $T_{cruise} \approx 0.001969s^2 + 3.369s + 51.54$ | Fig. 6-(b) |
| $H_{cruise} \approx -0.03124s^2 + 30.24s + 130.9$ | Fig. 6-(c) |
| $T_{descent} \approx -0.002829s^2 + 3.6802s - 361.6$ | Fig. 6-(d) |

TABLE VIII
STANDARD PARAMETERS CONSIDERED FOR THE MISSION PROFILE ANALYSIS AND THE AERODYNAMIC MODELING [28]–[30]

| $L/D$ | $L$ | $D$ | $\mu$ | $\rho$ | $g$ |
|---|---|---|---|---|---|
| 15 | 0.18 | 0.012 | 0.02 | $1.29\,\mathrm{kg/m^3}$ | $9.81\,\mathrm{m/s^2}$ |

model is provided in the following subsection, Section IV-A.

## IV. AIRCRAFT POWERTRAIN MODELING

This section briefly describes the aerodynamic basics influencing an aircraft's propulsion power before presenting the all-electric aircraft powertrain modeling, encompassing all key components.

### A. Generation of Aerodynamic Forces

Fig. 9 presents a free-body diagram of the forces acting on a tilted and leveled aircraft: weight ($W$), lift ($L$), drag ($D$), and thrust ($F$). Lift is generated through the differential in airflow pressure created by the speed above and below the wings. Eq. (1) describes the magnitude of the lift force perpendicular to the flight direction. The aircraft's weight ($W$) opposes the lift ($L$). Both are in equilibrium during cruising. The same holds for the aircraft's thrust force ($F$) that overcomes the drag force ($D$) of the aircraft described by eq. (2).

$$L = \frac{1}{2}\rho C_L S v^2 \approx K_a v^2 \tag{1}$$

$$D = \frac{1}{2}\rho C_D S v^2 \approx \frac{K_a v^2}{L/D} \tag{2}$$

Dividing eq. (1) by eq. (2), yields eq. (3), implying that the lift-to-drag ratio ($L/D$) is determined solely by the coefficients.

$$\frac{L}{D} = \frac{C_L}{C_D} \tag{3}$$

The $L/D$-ratio is a crucial metric for evaluating aircraft efficiency. Raymer (2018) presents a range of standard L/D-ratios [31], which typically falls between 15 and 20 for civil jets, while for retractable propeller aircraft, it is around 14.

Force calculations are done for each flight phase as follows.

*1) Cruising:* Cruising is represented by the leveled aircraft in Fig. 9-(a). The lift force ($L$) in eq. (1) is equal to the weight of the aircraft, $W = mg$, and the drag force ($D$) in eq. (2) is equal to the aircraft's thrust force ($F$). By dividing eq. (1) by eq. (2), the thrust can be estimated as

$$F = \frac{m_{tot} g}{{}^{L}\!/_{D}}. \tag{4}$$

*2) Climb and Descent:* Similarly, climb and descent are described by the tilted aircraft in Fig. 9-(b), where the thrust force ($F$) can be expressed as

$$F = m_{tot} g \left( \sin(\theta) + \frac{1}{{}^{L}\!/_{D}} \cos(\theta) + \frac{a}{g} \right), \tag{5}$$

where the sine term is negative during descent.

*3) Takeoff and Taxiing:* The aircraft's thrust force ($F$) is influenced by the ground contact during takeoff and taxiing, which could be modeled according to eq. (6).

$$F = m_{tot} g \left( \mu \left[ 1 - \frac{L}{m_{tot} g} \right] + \frac{D}{m_{tot} g} + \frac{a}{g} \right). \tag{6}$$

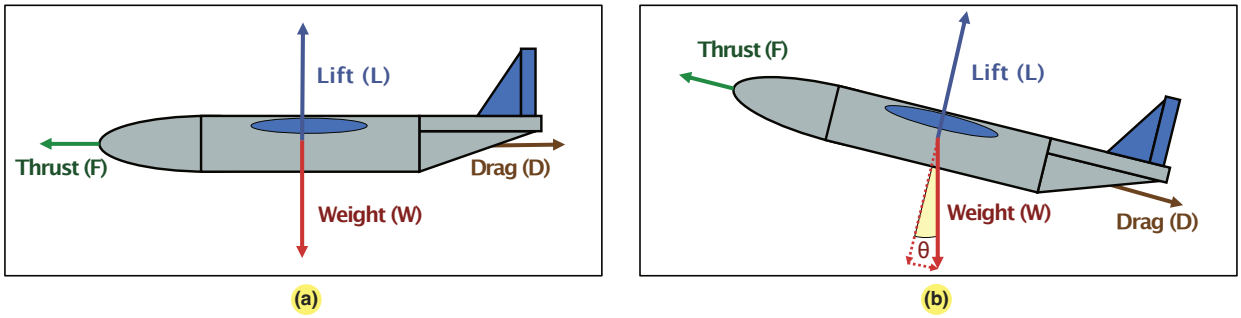


Fig. 9. Free body diagram showing the forces acting on the aircraft body. **(a):** Leveled aircraft. **(b):** Tilted aircraft.

In eq. (6), both the lift ($L$) and the drag ($D$) are proportional to the velocity squared. The takeoff speed ($v_{takeoff}$) occurs when lift ($L$) is equal to the aircraft weight, implying that

$$\frac{m_{tot}g}{v_{takeoff}^2} \approx \frac{1}{2}\rho C_L S = K_a \tag{7}$$

In the case of Dash-8 Q100, $K_a = 61.2\,\mathrm{kg/m}$. By applying eq. (7), the thrust in eq. (6) can be estimated as

$$F = m_{tot}g\left(\mu\left[1-\left(\frac{v}{v_{takeoff}}\right)^2\right]+\frac{1}{L/D}\left(\frac{v}{v_{takeoff}}\right)^2+\frac{a}{g}\right). \tag{8}$$

### B. Aircraft Weight Calculation

The weight of a conventional aircraft is calculated by summing its three main components: empty weight ($m_0$), fuel weight ($m_f$), and payload weight ($m_{pl}$), as outlined in eq. (9).

$$m_{tot} = m_0 + m_f + m_{pl} \tag{9}$$

The empty weight of an aircraft includes its structure, interior, and technical equipment like landing gear, and remains constant. In contrast, fuel and payload weights vary with different missions. Fuel weight depends on flight duration and conditions, while payload weight accounts for passengers or cargo. Notably, in battery-electric aircraft, unlike conventional ones, fuel weight remains constant during flight. Therefore, the total weight mainly varies with the payload, and the electric system's weight is part of the empty weight. The calculation for the total weight of electric aircraft, considering the weight of each electrical component ($m_i$), is given in eq. (10).

$$m_{tot} = m_0 + m_{pl} + \sum_{i=1}^{n} m_i \tag{10}$$

### C. Power and Energy Requirement

The power required at any time is calculated by multiplying the aircraft's thrust force by its velocity. Formulas for power requirements in different flight phases are detailed in Table IX, using eqs. (4), (5), and (8). The aircraft's powertrain is dimensioned by the highest power requirement in any flight phase, as mathematically represented in eq. (11).

$$P_{prop} = max\Big\{P_{takeoff}, P_{climb}, P_{cruise}, P_{descent}\Big\} \tag{11}$$

TABLE IX
POWER REQUIRED DURING THE DIFFERENT PHASES OF THE FLIGHT

| Phase of flight | Equation |
|---|---|
| 0. Takeoff | $P_{takeoff} = m_{tot}g\left(\mu\left[1-\left(\frac{v}{v_{takeoff}}\right)^2\right]+\frac{1}{L/D}\left(\frac{v}{v_{takeoff}}\right)^2+\frac{a}{g}\right)v$ |
| 1. Climb | $P_{climb} = m_{tot}g\left(\sin(\theta)+\frac{1}{L/D}\cos(\theta)+\frac{a}{g}\right)v$ |
| 2. Cruise | $P_{cruise} = m_{tot}g\left(\frac{1}{L/D}\right)v$ |
| 3. Descent | $P_{descent} = m_{tot}g\left(\sin(\theta)+\frac{1}{L/D}\cos(\theta)+\frac{a}{g}\right)v$ |

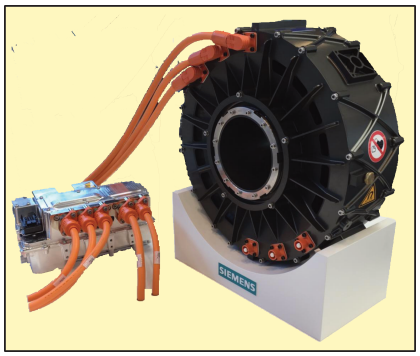


Fig. 10. Demonstration prototype of the Siemens SP260D-A [32] representative motor.

The energy requirement is determined by the total power consumption during flight, which can be calculated by integrating the power over the flight time, as shown in eq. (12).

$$\begin{aligned} E_{tot} = &\int_0^{t_0} P_{takeoff}\ dt + \int_{t_0}^{t_1} P_{climb}\ dt \\ &+ \int_{t_1}^{t_2} P_{cruise}\ dt + \int_{t_2}^{t_3} P_{descent}\ dt \end{aligned} \tag{12}$$

TABLE X
SPECIFICATION OF SIEMENS SP260D-A DIRECT-DRIVE, AXIAL FLUX, AEROSPACE-GRADE PM MOTOR WITH REDUNDANT 3-PHASE WINDINGS [32]

| Continuous power | Nominal torque | Rated speed | Efficiency | Active mass | Power density | Torque density | DC supply | Cooling |
|---|---|---|---|---|---|---|---|---|
| 260 kW | 977 Nm | 2500 rpm | $\geq 95\,\%$ | 44 kg | 5.9 kW/kg | 22.2 Nm/kg | 580 V | Oil @ 90 °C |

TABLE XI
REPRESENTATIVE VOLTAGE RATINGS OF EACH COMPONENT IN THE ELECTRIC POWERTRAIN (EPS) [32], [34]

| Battery | Battery breaker | Converter | Primary cable | DC-link | Primary breaker | Primary inverter | Electric motor |
|---|---|---|---|---|---|---|---|
| 800 $V_{dc}$ | 800 $V_{dc}$ | 800 $V_{dc}$ / 600 $V_{dc}$ | 600 $V_{dc}$ | 580 $V_{dc}$ | 580 $V_{dc}$ | 580 $V_{dc}$ / 410 $V_{rms}$ | 410 $V_{rms}$ |

TABLE XII
BASE CASE FOR THE CONSIDERED COMPONENT-LEVEL ENERGY AND POWER DENSITIES [35]

| $e_{bat}$ | $p_{bat}$ | $p_{mot}$ | $p_{inv}$ | $p_{conv}$ | $p_{cb1}$ | $p_{cb2}$ | $k_{bat}$ |
|---|---|---|---|---|---|---|---|
| 0.22 kWh/kg | 0.80 kW/kg | 5.90 kW/kg | 9.00 kW/kg | 2.50 kW/kg | 67.50 kW/kg | 34.00 kW/kg | 0.80 |

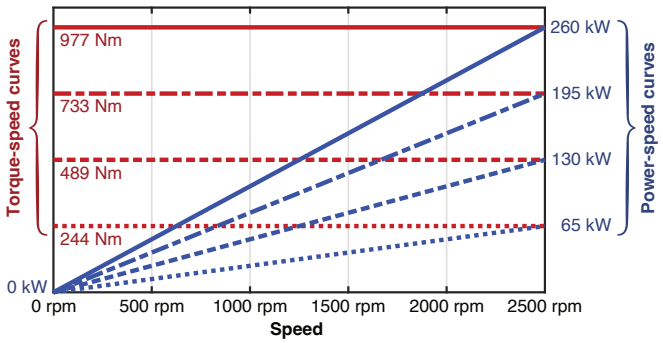


Fig. 11. Torque-speed and power-speed characteristic curves of the Siemens SP260D-A motor with constant torque region and no flux-weakening region.

### D. Powertrain Sizing Model

For this study, the Siemens SP260D-A (see Fig. 10) is chosen as a representative aerospace-grade motor, with rated performance specifications given in Table X and power-torque-speed characteristics in Fig. 11. The motor is selected due to its high power density at a low rotational speed, its efficiency, and its three-phase redundant armature windings. Rolls-Royce has a similar motor for commuter aircraft applications [33]. To comply with Siemens SP260D-A specifications, Table XI lists representative voltage ratings for all the primary components in the electric propulsion system (EPS). Fig. 12 depicts the EPS components, where the electric motor represents the mechanical output of the EPS.

Fig. 13 illustrates all the power flows of the EPS and the interaction with the TMS. The efficiencies of both the EPS and TMS are given in eq. (13), and the associated heat losses are calculated in eq. (14).

$$\begin{aligned} \eta_{tms} &= \eta_{bat}\eta_{cb2}\eta_{conv}\eta_{cab}\eta_{cb1}\eta_{inv} \\ \eta_{eps} &= \eta_{bat}\eta_{cb2}\eta_{conv}\eta_{cab}\eta_{cb1}\eta_{inv}\eta_{mot}\eta_{prop} \end{aligned} \tag{13}$$

$$\begin{aligned} \dot{Q}_{tot} = \dot{Q}_{gear} + \dot{Q}_{mot} + \dot{Q}_{cb1} + \dot{Q}_{cb2} + \dot{Q}_{inv1} + \dot{Q}_{inv2} \\ + \underbrace{\dot{Q}_{cab1} + \dot{Q}_{cab2}}_{\dot{Q}_{cab}} + \dot{Q}_{conv} + \dot{Q}_{bcb} + \dot{Q}_{bat} \end{aligned} \tag{14}$$

Tables XII, XIII, and XIV present detailed data on power densities, performances, and efficiencies for the EPS and TMS. While Chin *et. al.* (2020) report a battery efficiency as low as 90 % for smaller urban aircraft [40], Lammen and Vankan (2020) find a 92.5 % battery efficiency for single-aisle aircraft [39], which we select for this study. Table XV details a procedure for sizing the EPS and TMS, where the TMS circuit size is based on heat losses. Due to very strict requirements on the battery's maximum operating temperature (35 °C), the thermal management is more demanding for the battery than for the power train components. Consequently, the battery TMS (BTMS) is dimensioned separately from the other power train components (PTMS), as illustrated in Fig. 13. The BTMS is dimensioned to remove the battery heat load $\dot{Q}_{bat}$, and the PTMS is dimensioned to remove the other heat loads Two parameters are used to dimension each TMS system: $h_{<b/p>tms}$, describing the power consumed by the TMS per kW of heat removed, and $p_{<b/p>tms}$, describing the amount of heat removed per kg of TMS. The BTMS mass sizing equation, adopted from Kellermann *et. al.* (2022) [37], requires an extra term to cancel the added battery mass. This has to do with how the authors accounted for the increase in battery mass that resulted from the BTMS power consumption. This explains the second term in the expression for $m_{btms}$ in step #7 in Table XV.

### E. Dimensioning of Energy Storage

The battery's energy, power, and weight are based on specified requirements. Its power consumption is the sum of the TMS circuit and the EPS usage. Energy requirements include the total power needed during flight and necessary reserves. A key consideration is the battery's allowable discharge, dictated by the factor $k_{bat}$, as indicated in eq. (15).

$$\begin{aligned} E_{bat} &= \int_0^{t_3} \frac{P_{bat}(t)}{k_{bat}} dt + \frac{P_{cruise}}{\eta_{eps}} \Delta T_{res} \\ &\approx \frac{E_{tot}}{\eta_{eps} k_{bat}} + \frac{P_{cruise}}{\eta_{eps}} \Delta T_{res} \end{aligned} \tag{15}$$

The last part of eq. (15) approximates battery requirements, excluding TMS power needs, and uses $E_{tot}$ from eq. (12). For thorough analysis, all power requirements, as listed in Table

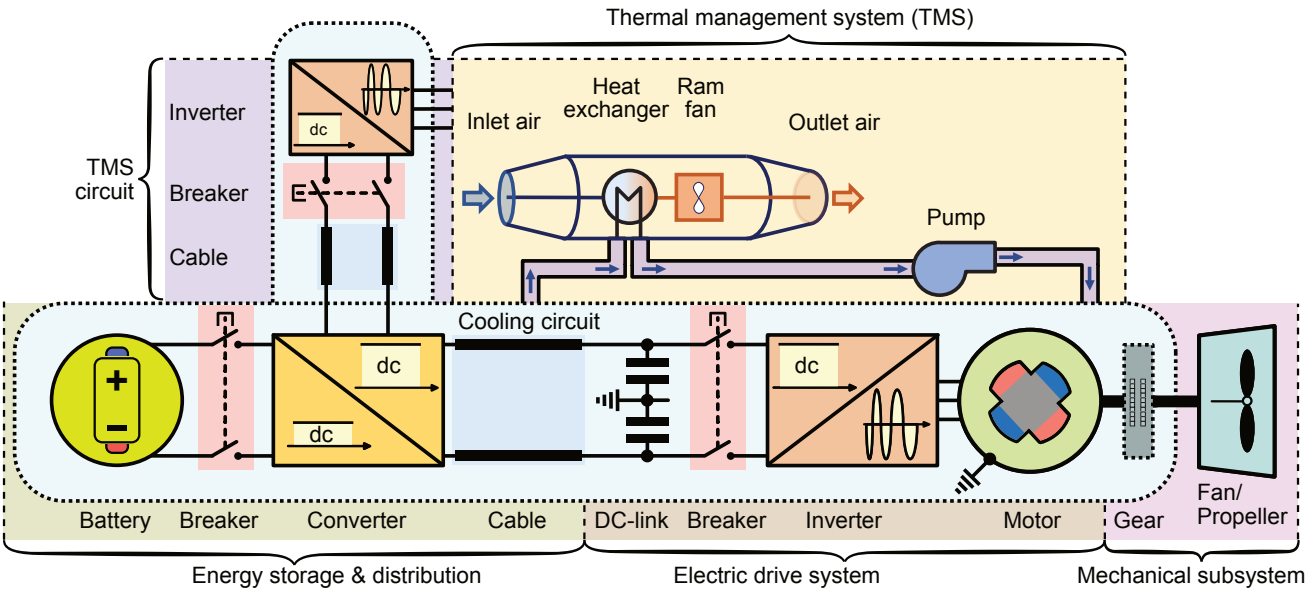


Fig. 12. Overview for the electric propulsion system (EPS) onboard the commuter aircraft. The system is separated into an EPS and TMS circuit, while the battery, DC/DC converter, and battery breaker are shared by the circuits.

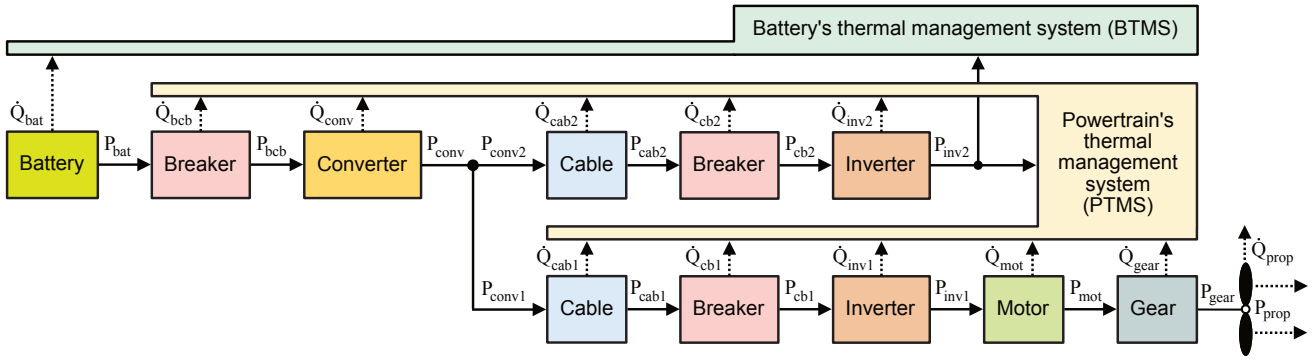


Fig. 13. Overview of power flows and losses in the electric propulsion system (EPS) to be absorbed by the thermal management system (TMS).

TABLE XIII
BASE CASE FOR THE THERMAL MANAGEMENT PERFORMANCES [36], [37], CABLING CONSTRAINTS AND GEAR MASS

| $p_{btms}$ | $h_{btms}$ | $p_{ptms}$ | $h_{ptms}$ | $u_{dc}$ | $i'_{cab}$ | $l_{cab1} \approx w$ | $l_{cab2} \approx l$ | $k_{gear}$ |
|---|---|---|---|---|---|---|---|---|
| 0.21 kW/kg | 1.66 kW/kW | 0.83 kW/kg | 0.14 kW/kW | 580.0 V | 100.0 A/kg/m | 14 m or 23 m | 11.8 m or 14.5 m | 0.25 |

TABLE XIV
BASE CASE FOR THE CONSIDERED COMPONENT-LEVEL EFFICIENCIES [17], [38], [39]

| $\eta_{bat}$ | $\eta_{mot}$ | $\eta_{inv}$ | $\eta_{conv}$ | $\eta_{cb1}$ | $\eta_{cb2}$ | $\eta_{cab}$ | $\eta_{gear}$ | $\eta_{prop}$ |
|---|---|---|---|---|---|---|---|---|
| 92.5 % | 95.0 % | 96.0 % | 96.0 % | 99.2 % | 99.2 % | 99.6 % | 99.0 % | 89.0 % |

XV, should be considered, with detailed sizing calculations provided in Appendix A. The battery's primary roles are to provide power capacity and energy storage for the entire flight. Its weight is based on whichever of these two functions is more demanding, as specified in eq. (16).

$$m_{bat} = max\left\{\frac{E_{bat}}{e_{bat}}, \frac{P_{bat}}{p_{bat}}\right\} \tag{16}$$

The equations listed in Table XV emphasize the interdependence of system components. The battery weight depends on the power needs of both the TMS and EPS, meaning increased requirements lead to a heavier battery, consequently raising the overall power demands and the weight of the TMS and EPS.

## V. Results and Discussion

This section presents the outcomes of the powertrain sizing model and mission profile scenarios, utilizing the normalized mission profile to estimate the power and energy needs across various flight routes.

TABLE XV
EQUATIONS USED TO SIZE THE EPS AND THE TMS.

| Step | Component | Power | Mass | Heat loss |
|---|---|---|---|---|
| #1 | Gear | $P_{gear} = {}^{P_{prop}}/_{\eta_{prop}}$ | $m_{gear} = {}^{k_{gear} P_{mot}^{0.76} n_{mot}^{0.13}}/_{n_{gear}^{0.89}}$ | $\dot{Q}_{gear} = (1/\eta_{gear} - 1) P_{gear}$ |
| #2 | Electric motor | $P_{mot} = {}^{P_{gear}}/_{\eta_{gear}}$ | $m_{mot} = {}^{P_{mot}}/_{p_{mot}}$ | $\dot{Q}_{mot} = (1/\eta_{mot} - 1) P_{mot}$ |
| #3 | Primary inverter | $P_{inv1} = {}^{P_{mot}}/_{\eta_{mot}}$ | $m_{inv1} = {}^{P_{inv1}}/_{p_{inv}}$ | $\dot{Q}_{inv1} = (1/\eta_{inv} - 1) P_{inv1}$ |
| #4 | Primary breaker | $P_{cb1} = {}^{P_{inv1}}/_{\eta_{inv}}$ | $m_{cb1} = {}^{P_{cb1}}/_{p_{cb1}}$ | $\dot{Q}_{cb1} = (1/\eta_{cb1} - 1) P_{cb1}$ |
| #5 | Primary cable | $P_{cab1} = {}^{P_{cb1}}/_{\eta_{cb1}}$ | $m_{cab1} = {}^{P_{cab1} l_{cab1}}/_{u_{dc} i'_{cab}}$ | $\dot{Q}_{cab1} = (1/\eta_{cab} - 1) P_{cab1}$ |
| #6 | Converter (part 1) | $P_{conv1} = {}^{P_{cab1}}/_{\eta_{cab}}$ | $m_{conv1} = {}^{P_{conv1}}/_{p_{conv}}$ | $\dot{Q}_{conv1} = (1/\eta_{conv} - 1) P_{conv1}$ |
| #7 | Battery TMS | $P_{btms} = h_{btms} \dot{Q}_{bat}$ | $m_{btms} = {}^{\dot{Q}_{bat}}/_{p_{btms}} - {}^{P_{btms}}/_{0.69}$ | |
| #8 | Powertrain TMS | $P_{ptms} = h_{ptms}(\dot{Q}_{tot} - \dot{Q}_{bat})$ | $m_{ptms} = {}^{(\dot{Q}_{tot} - \dot{Q}_{bat})}/_{p_{ptms}}$ | |
| #9 | Auxiliary inverter | $P_{inv2} = P_{btms} + P_{ptms}$ | $m_{inv2} = {}^{P_{inv2}}/_{p_{inv}}$ | $\dot{Q}_{inv2} = (1/\eta_{inv} - 1) P_{inv2}$ |
| #10 | Auxiliary breaker | $P_{cb2} = {}^{P_{inv2}}/_{\eta_{inv}}$ | $m_{cb2} = {}^{P_{cb2}}/_{p_{cb2}}$ | $\dot{Q}_{cb2} = (1/\eta_{cb2} - 1) P_{cb2}$ |
| #11 | Auxiliary cable | $P_{cab2} = {}^{P_{cb2}}/_{\eta_{cb1}}$ | $m_{cab2} = {}^{P_{cab2} l_{cab2}}/_{u_{dc} i'_{cab}}$ | $\dot{Q}_{cab2} = (1/\eta_{cab} - 1) P_{cab2}$ |
| #12 | Converter (part 2) | $P_{conv2} = {}^{P_{cab2}}/_{\eta_{cab}}$ | $m_{conv2} = {}^{P_{conv2}}/_{p_{conv}}$ | $\dot{Q}_{conv2} = (1/\eta_{conv} - 1) P_{conv2}$ |
| #13 | Converter (total) | $P_{conv} = P_{conv1} + P_{conv2}$ | $m_{conv} = {}^{P_{conv}}/_{p_{conv}}$ | $\dot{Q}_{conv} = (1/\eta_{conv} - 1) P_{conv}$ |
| #14 | Battery breaker | $P_{bcb} = {}^{P_{conv}}/_{\eta_{conv}}$ | $m_{bcb} = {}^{P_{bcb}}/_{p_{cb2}}$ | $\dot{Q}_{bcb} = (1/\eta_{cb2} - 1) P_{bcb}$ |
| #15 | Battery | $P_{bat} = {}^{P_{bcb}}/_{\eta_{cb2}}$ | $m_{bat} \geq {}^{P_{bat}}/_{p_{bat}}$ | $\dot{Q}_{bat} = (1/\eta_{bat} - 1) P_{bat}$ |

### A. Base Case Analysis

This study's base case analyzes current EPS technologies (referenced in Tables XII-XIV) to assess their capability to fulfill the power and energy requirements for different routes, focusing on the P-Volt and ES-19 aircraft. Fig. 14 depicts component weight calculations for meeting these demands. The results show that the two shortest routes are closest to becoming achievable based on technical performances. As the distances increase, so does the weight. For the longest route (Route 4), the weight limits from Tables III and IV are exceeded by $101.5\,\%$ and $124.7\,\%$, respectively. However, including additional weight allocated for diversion energy storage, the total weight exceeds the requirement by $199.0\,\%$ and $548.7\,\%$, respectively. The additional weight for reserve energy on the shortest flights is smaller because these distances are power-dimensioned, not energy-dimensioned, as are the longer routes.

The necessity of diversion energy reserves as mandated by safety regulations poses a substantial challenge in aviation. Both the FAA (Federal Aviation Administration) and EASA (European Union Aviation Safety Agency), the authoritative entities for American and European civil aviation respectively, set a minimum requirement of 30 minutes fuel reserves under VFR (Visual Flight Rules) and 45 minutes under IFR (Instrument Flight Rules) conditions. The latter is required when the conditions render the pilot unable to see the landscape, for example, during night flights or when experiencing fog or other bad weather. Adding these requirements to the base scenarios results in significant weight gains, as shown in Fig 14, where the VFR regulations are applied to the base scenarios. This underscores the importance of including this mandatory requirement when sizing an electric aircraft. It could be a part of the reason that Heart Aerospace transitioned from the ES-19 to the ES-30 using biofuel generators for the reserve requirements.

### B. Power-Dimensioning vs. Energy-Dimensioning

By utilizing the normalized mission profile for all possible flight distances, it can be seen in Fig. 15 that there is a transitional point where each aircraft changes from being power-dimensioned to being energy-dimensioned. It is important to note that for shorter flights, the battery's power is the limiting factor, whereas, for longer flights, it is the energy. Our research highlights the importance of considering the power required for takeoff and climb to size the propulsion system accurately. Ignoring the power requirement during the takeoff could significantly underestimate the batteries for shorter flights. As depicted in Fig. 15, the battery mass remains constant for distances up to $88.5\,\mathrm{km}$ for the P-Volt and up to $134\,\mathrm{km}$ for the ES-19, illustrating the significance of this transition point.

### C. Sensitivity Analysis

The influence on total aircraft weight is scrutinized through a sensitivity analysis conducted for both the P-Volt and ES-19, using the $149\,\mathrm{km}$ Bodø to Stokmarknes route (Route 3) as the reference. This analysis explores how variations in component performance metrics impact the overall aircraft weight. Results, illustrated in Figs. 16 and 17, pinpoint where enhancement efforts should be concentrated. The sensitivity scenarios are categorized into two groups: one assessing the effect of improvements in component efficiency, and the other examining changes in critical parameters like specific energy, specific power, voltage level, empty weight, and aircraft range.

The sensitivity analysis results show similar results for the P-volt and the ES-19, even though there are slightly bigger total weight changes for performance improvements on the ES-19. In general, improvements to the specific power of the smaller components show little effect on the total aircraft weight, while parameters such as battery specific energy, aircraft range, and aircraft empty weight have significant effects. Both range and empty weight increase the overall weight linearly, while increasing the battery's specific energy lowers the total weight linearly. In particular, a $10\,\%$ increase in battery energy density $220\,\mathrm{Wh/kg}$ to $242\,\mathrm{Wh/kg}$, reduces the aircraft weight by about $6\,\%$ for both cases.

Improvements in component efficiency are shown in Fig. 17 to have a more significant effect on the system. An increase in efficiency of $1\,\%$ for either of the components yields $1\,\%$ to $2\,\%$ in total weight reduction. For the battery, every $1\,\%$

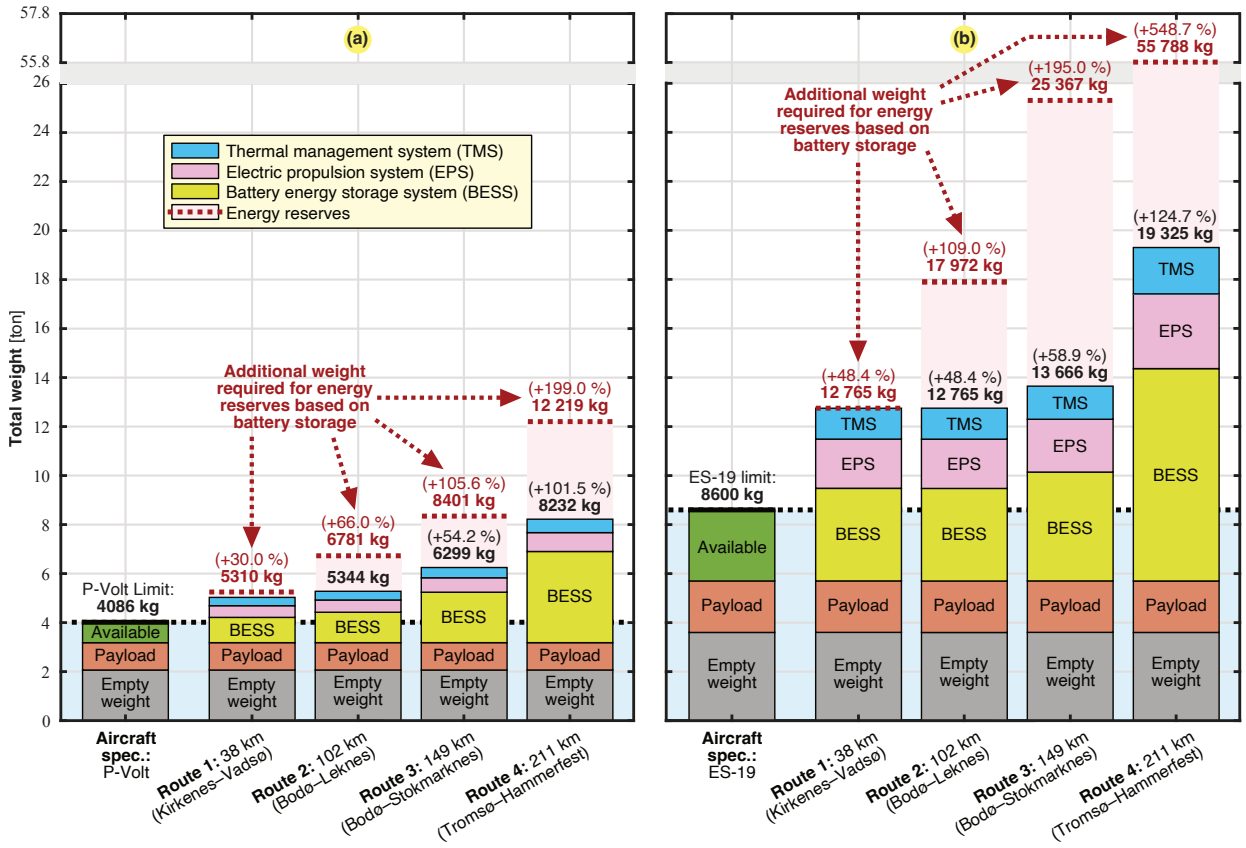


Fig. 14. An overview of weight distribution for the investigated routes, including VFR regulations. **(a):** P-Volt aircraft. **(b):** ES-19 aircraft.

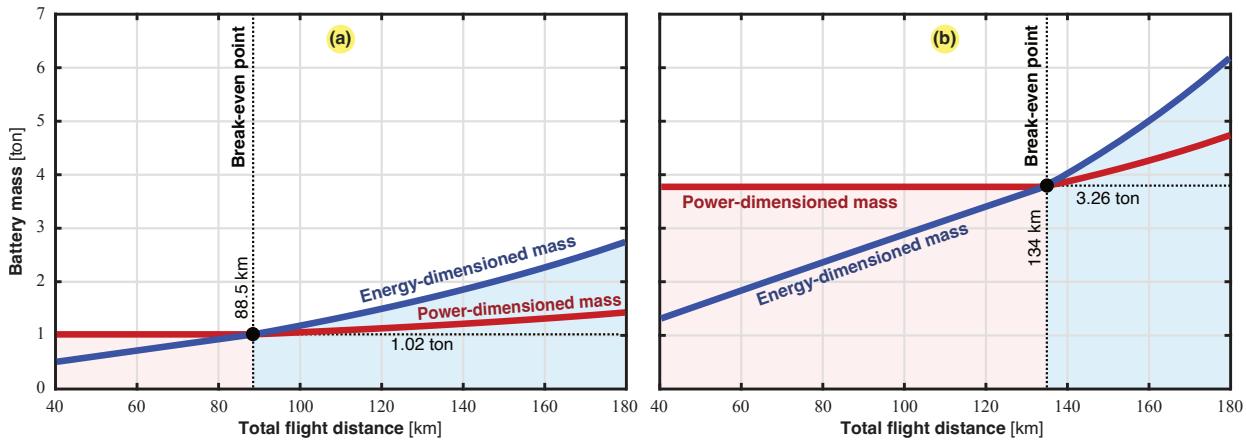


Fig. 15. Power-dimensioned battery mass versus energy-dimensioned mass as a function of total flight distance utilizing the generalized mission profile estimated and presented in Fig. 8. **(a):** P-Volt aircraft. **(b):** ES-19 aircraft. Note that this is without the energy reserve requirements.

efficiency improvement reduces the total weight by 2 % to 3 %. A minor effect is seen for the components furthest downstream of the battery, with the motor being the most significant and the converter the least significant.

The sensitivity analysis should be considered in relation to Route 3 results presented in Fig. 14, which shows the necessity of reducing the aircraft weight with 35.1 % and 37.1 % for the P-Volt and ES-19, respectively. Fig. 17 shows the necessity of improving the efficiency of every part of the system. There is no silver bullet; major improvements in a single component will not be enough to reach the target weights of the aircraft. However, significant weight reductions can be achieved with a combination of minor improvements in component efficiencies. Nevertheless, the aircraft's structural weight and the battery's specific energy are highly influential.

The weight-sharing distribution among the various components of an all-electric powertrain is a crucial factor. As illustrated in Fig. 14, battery storage commands an increasingly dominant weight proportion for extended routes and larger aircraft. Specifically, for Route 4 and the ES-19, the battery's share exceeds 50 %, indicating a majority. The worked example presented in the appendix provides more details.

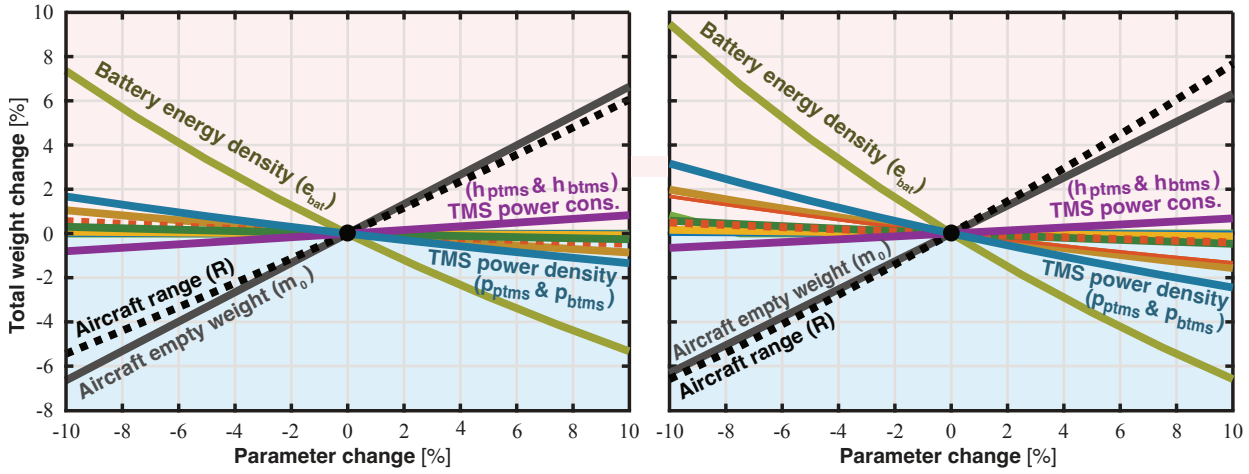


Fig. 16. Sensitivity of the total aircraft weight as a function of specific energy and specific power of the components for Route 3 (149 km). Additionally, aircraft range, voltage level, and empty weight of the aircraft are included. **(a):** P-Volt aircraft. **(b):** ES-19 aircraft.

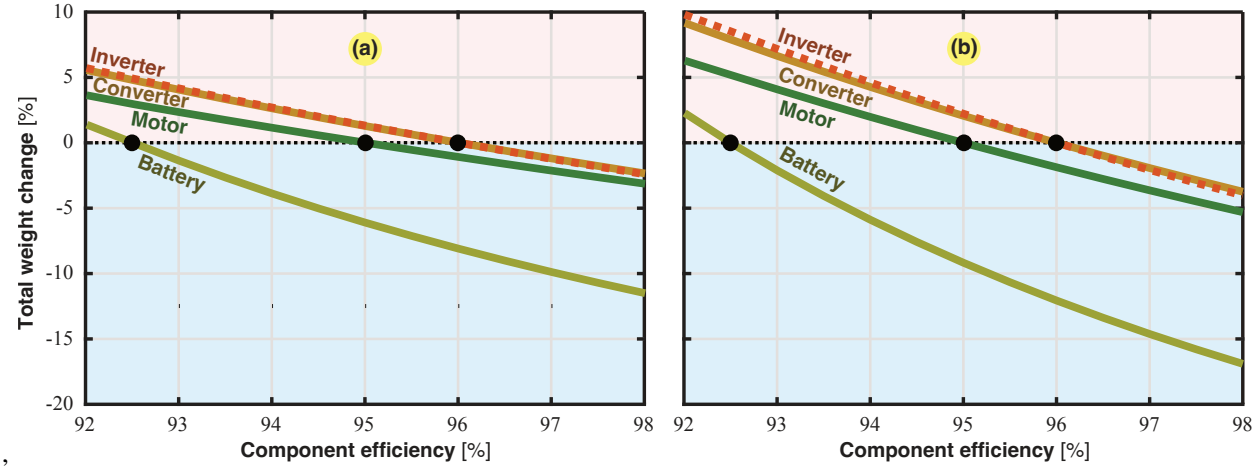


Fig. 17. Sensitivity of the total aircraft weight as a function of component efficiencies for Route 3 (149 km). **(a):** P-Volt aircraft. **(b):** ES-19 aircraft.

## VI. Conclusion

This paper evaluates the viability of electrifying Norway's short-haul route network with two all-electric commuter aircraft designs: the 19-seater Heart Aerospace ES-19 and the 9-seater Tecnam P-Volt. The work is supported by statistical analysis of real-world data from 1500 flights. Findings reveal that cruising power constitutes about 43 % of takeoff power, and shorter missions experience significantly longer climb and descent times. The following insights should be emphasized.

1) The shortest missions are dimensioned by output power rather than energy storage capability. This trend persists for distances up to 88.5 km for the P-Volt and extends to 134 km for the ES-19;
2) In scenarios where the propulsion system is power-dimensioned, it inherently possesses surplus energy, thereby diminishing the need for additional diversion energy reserves. Notably, for the shortest route involving the ES-19, this surplus negates the requirement for any extra energy reserve;
3) For the longest flight, factoring in the diversion energy reserve results in a 48 % total weight increase for the P-Volt and a more substantial 188 % surge for the ES-19. This underscores the nonlinear nature of powertrain sizing, where added mass creates additional energy needs, particularly pronounced in larger aircraft models;
4) Enhancements in the energy efficiency of powertrain components significantly outweigh the benefits of improving their power density. Gains in efficiency lead to a more substantial reduction in overall mass compared to merely decreasing the mass of the components. However, reducing the mass of the battery stands as a notable exception, yielding effects comparable to those achieved through efficiency improvements.

Among the four routes studied, i.e., 38 km, 102 km, 149 km, and 211 km, the shortest trip is closest to become achievable with today's technology performance. In general, the results highlight significant challenges in scaling up all-electric commuter aircraft with battery-based energy storage. Additional redundancy requirements further intensify the complexity of adhering to aircraft weight constraints.

The appendix includes worked examples of sizing the propulsion systems of the P-Volt and the ES-19, based on their announced base designs of 2× 320 kW and 4× 400 kW output

TABLE XVI
POWER-BASED POWERTRAIN SIZING OF THE REFERENCE AIRCRAFT'S ANNOUNCED DESIGNS BASED ON TABLES XII, XIII, AND XIV.

| | | Efficiency | Power input | Heat loss | Power output | Power density | Mass |
|---|---|---|---|---|---|---|---|
| Battery | P-Volt | 92.50 % | 971.1 kW | 72.8 kW | 898.3 kW | 0.80 kW/kg | 1122.9 kg |
| | ES-19 | —— " —— | 2425.9 kW | 181.9 kW | 2244.0 kW | —— " —— | 2805.0 kg |
| Battery breaker | P-Volt | 99.20 % | 898.3 kW | 7.2 kW | 891.1 kW | 34.00 kW/kg | 26.2 kg |
| | ES-19 | —— " —— | 2244.0 kW | 18.0 kW | 2226.0 kW | —— " —— | 65.5 kg |
| Converter | P-Volt | 96.00 % | 891.1 kW | 35.6 kW | 855.5 kW | 2.50 kW/kg | 342.2 kg |
| | ES-19 | —— " —— | 2226.0 kW | 89.0 kW | 2137.0 kW | —— " —— | 854.8 kg |
| Auxiliary cable | P-Volt | 99.60 % | 145.2 kW | 0.6 kW | 144.6 kW | 4.92 kW/kg | 29.4 kg |
| | ES-19 | —— " —— | 362.8 kW | 1.4 kW | 361.4 kW | 4.00 kW/kg | 90.4 kg |
| Auxiliary breaker | P-Volt | 99.20 % | 144.6 kW | 1.2 kW | 143.4 kW | 67.50 kW/kg | 2.1 kg |
| | ES-19 | —— " —— | 361.4 kW | 2.9 kW | 358.5 kW | —— " —— | 5.3 kg |
| Auxiliary inverter | P-Volt | 96.00 % | 143.4 kW | 5.7 kW | 137.7 kW | 9.00 kW/kg | 15.3 kg |
| | ES-19 | —— " —— | 358.5 kW | 14.3 kW | 344.2 kW | —— " —— | 38.2 kg |
| Battery TMS | P-Volt | 1.66 kW/kW | 120.8 kW | −72.8 kW | 0.0 kW | 0.21 kW/kg | 171.6 kg |
| | ES-19 | —— " —— | 302.0 kW | −181.9 kW | 0.0 kW | —— " —— | 428.5 kg |
| Powertrain TMS | P-Volt | 0.14 kW/kW | 16.9 kW | −120.6 kW | 0.0 kW | 0.83 kW/kg | 145.3 kg |
| | ES-19 | —— " —— | 42.2 kW | −301.2 kW | 0.0 kW | —— " —— | 362.9 kg |
| Primary cable | P-Volt | 99.60 % | 710.3 kW | 2.8 kW | 2×353.7 kW | 4.14 kW/kg | 170.9 kg |
| | ES-19 | —— " —— | 1775.6 kW | 7.1 kW | 4×442.1 kW | 2.52 kW/kg | 701.8 kg |
| Primary breaker | P-Volt | 99.20 % | 2×353.7 kW | 5.7 kW | 2×350.9 kW | 67.50 kW/kg | 10.4 kg |
| | ES-19 | —— " —— | 4×442.1 kW | 14.1 kW | 4×438.6 kW | —— " —— | 26.0 kg |
| Primary inverter | P-Volt | 96.00 % | 2×350.9 kW | 28.1 kW | 2×336.8 kW | 9.00 kW/kg | 74.9 kg |
| | ES-19 | —— " —— | 4×438.6 kW | 70.2 kW | 4×421.0 kW | —— " —— | 187.1 kg |
| Electric motor | P-Volt | 95.00 % | 2×336.8 kW | 33.7 kW | 2×320.0 kW | 5.90 kW/kg | 108.5 kg |
| | ES-19 | —— " —— | 4×421.0 kW | 84.2 kW | 4×400.0 kW | —— " —— | 271.2 kg |
| Overall system | P-Volt | 65.90 % | 971.1 kW | 330.4 kW | 2×320.0 kW | 0.29 kW/kg | 2219.7 kg |
| | ES-19 | 65.95 % | 2425.9 kW | 825.7 kW | 4×400.0 kW | 0.27 kW/kg | 5836.7 kg |

TABLE XVII
VERIFICATION OF P-VOLT'S SYSTEM-LEVEL EFFICIENCY AND POWER DENSITY AGAINST APPROXIMATIONS

| | | Efficiency | Power density |
|---|---|---|---|
| This work | Table XVI | 65.90 % | 0.27 kW/kg |
| Approximation | Eqs. (17) & (18) | ≤ 79.38 % | ≤ 0.45 kW/kg |

power, respectively. Additionally, the calculations are semi-analytically verified through a comparative analysis of system-level efficiency and power density against approximations.

## APPENDIX
## WORKED EXAMPLE AND VERIFICATION

A worked example of power, heat, and mass values of all components for the announced base designs of the 9-seater Tecnam P-Volt and 19-seater Heart Aerospace ES-19 are provided in Table XVI. The steps in Table XV are reiterated several times to reach an equilibrium. The overall mass of the powertrain exceeds the available weight by nearly three times for the P-Volt and two times for the ES-19. To verify the results, system-level efficiency and power density approximations in eqs. (17) and (18) can be considered. However, Table XVII shows that the more realistic values derived from this work are lower and caused by the thermal management system.

$$\eta_{tot} \leq \eta_{mot}\eta_{inv}\eta_{cb1}\eta_{cab}\eta_{conv}\eta_{cb2}\eta_{bat} \tag{17}$$

$$p_{tot} \leq \frac{1}{\frac{1}{p_{mot}} + \frac{1}{p_{inv}} + \frac{1}{p_{cb1}} + \frac{1}{p_{cab}} + \frac{1}{p_{conv}} + \frac{1}{p_{cb2}} + \frac{1}{p_{bat}}} \tag{18}$$

## REFERENCES


[1] G. Volker, A. Gangoli Rao, T. Grönstedt, C. Xisto, F. Linke, J. Melkert, J. Middel, B. Ohlenforst, S. Blakey, S. Christie, S. Matthes, and K. Dahlmann, "Evaluating the climate impact of aviation emission scenarios towards the paris agreement including COVID-19 effects," *Nat. Com.*, vol. 12, 06 2021.

[2] "Future of Aviation, *International Civil Aviation Organization (ICAO)*," https://www.icao.int/Meetings/FutureOfAviation/Pages/default.aspx.

[3] P. Strathoff, H. A. Savic, and E. Stumpf, "Performance comparison of conventional, hybrid-electric, and all-electric powertrains for small aircraft," in *Proc. AIAA Aviat. Forum*, 2020, p. 3252.

[4] D. S. Lee, G. Pitari, V. Grewe, K. Gierens, J. E. Penner, A. Petzold, M. Prather, U. Schumann, A. Bais, T. Berntsen *et al.*, "Transport impacts on atmosphere and climate: Aviation," *Atmos. Environ.*, vol. 44, no. 37, pp. 4678–4734, 2010.

[5] M. Lefèvre, A. Chaumond, P. Champelovier, L. G. Allemand, J. Lambert, B. Laumon, and A.-S. Evrard, "Understanding the relationship between air traffic noise exposure and annoyance in populations living near airports in france," *Environ. Int.*, vol. 144, p. 106058, 2020.

[6] H. Schefer, L. Fauth, T. H. Kopp, R. Mallwitz, J. Friebe, and M. Kurrat, "Discussion on electric power supply systems for all electric aircraft," *IEEE Access*, vol. 8, pp. 84 188–84 216, 2020.

[7] P. J. Ansell and K. S. Haran, "Electrified airplanes: A path to zero-emission air travel," *IEEE Electrif. Mag.*, vol. 8, no. 2, pp. 18–26, 2020.

[8] M. Ghassemi, A. Barzkar, and M. Saghafi, "All-electric NASA N3-X aircraft electric power systems," *IEEE Trans. Transp. Electrif.*, vol. 8, no. 4, pp. 4091–4104, 2022.

[9] T. P. Dever, K. P. Duffy, A. J. Provenza, P. L. Loyselle, B. B. Choi, C. R. Morrison, and A. M. Lowe, "Assessment of technologies for noncryogenic hybrid electric propulsion," National Aeronautics and Space Administration Cleveland, Tech. Rep., 2015.

[10] A. W. Schäfer, S. R. Barrett, K. Doyme, L. M. Dray, A. R. Gnadt, R. Self, A. O'Sullivan, A. P. Synodinos, and A. J. Torija, "Technological, economic and environmental prospects of all-electric aircraft," *Nat. Energy*, vol. 4, pp. 160–166, 2019.

[11] S. Sahoo, X. Zhao, and K. Kyprianidis, "A review of concepts, benefits, and challenges for future electrical propulsion-based aircraft," *Aerosp.*, vol. 7, no. 4, p. 44, 2020.

[12] M. T. Fard, J. He, H. Huang, and Y. Cao, "Aircraft distributed electric propulsion technologies—a review," *IEEE Trans. Transp. Electrif.*, vol. 8, no. 4, pp. 4067–4090, 2022.

[13] M. Hepperle, "Electric flight-potential and limitations," 2012. [Online]. Available: https://elib.dlr.de/78726/1/MP-AVT-209-09.pdf

[14] C. E. Riboldi and F. Gualdoni, "An integrated approach to the preliminary weight sizing of small electric aircraft," *Aerosp. Sci. Technol.*, vol. 58, pp. 134–149, 2016.

[15] C. E. Riboldi, F. Gualdoni, and L. Trainelli, "Preliminary weight sizing of light pure-electric and hybrid-electric aircraft," *Transp. Res. Procedia*, vol. 29, pp. 376–389, 2018.

[16] M. Armstrong, C. Ross, M. Blackwelder, and K. Rajashekara, "Propulsion system component considerations for NASA N3-X turboelectric distributed propulsion system," *SAE Int. J. Aerosp.*, vol. 121, no. 1, pp. 344–353, 2012.

[17] R. Jansen, C. Bowman, and A. Jankovsky, "Sizing power components of an electrically driven tail cone thruster and a range extender," in *Proc. AIAA Aviat. Technol. Integr. Oper. Conf.*, 2016, p. 3766.

[18] T. C. Cano, I. Castro, A. Rodríguez, D. G. Lamar, Y. F. Khalil, L. Albiol-Tendillo, and P. Kshirsagar, "Future of electrical aircraft energy power systems: An architecture review," *IEEE Trans. Transp. Electrif.*, vol. 7, no. 3, pp. 1915–1929, 2021.

[19] I. Staack, A. Sobron, and P. Krus, "The potential of full-electric aircraft for civil transportation: from the breguet range equation to operational aspects," *CEAS Aeronaut. J.*, vol. 12, pp. 803–819, 2021.

[20] A. R. Gnadt, R. L. Speth, J. S. Sabnis, and S. R. Barrett, "Technical and environmental assessment of all-electric 180-passenger commercial aircraft," *Prog. Aerosp. Sci.*, vol. 105, pp. 1–30, 2019.

[21] V. Marciello, M. Di Stasio, M. Ruocco, V. Trifari, F. Nicolosi, M. Meindl, B. Lemoine, and P. Caliandro, "Design exploration for sustainable regional hybrid-electric aircraft: A study based on technology forecasts," *Aerosp.*, vol. 10, no. 2, p. 165, 2023.

[22] M. A. Anker and J. K. Nøland, "Preliminary sizing of a battery-powered all-electric propulsion system for regional aircraft," in *Proc. Annu. Conf. IEEE Ind. Electron. Soc. (IECON)*, 2022, pp. 1–6.

[23] T. Bærheim, J. J. Lamb, J. K. Nøland, and O. S. Burheim, "Potential and limitations of battery-powered all-electric regional flights—A norwegian case study," *IEEE Trans. Transp. Electrif.*, vol. 9, no. 1, pp. 1809–1825, 2023.

[24] B. Jux, S. Foitzik, and M. Doppelbauer, "A standard mission profile for hybrid-electric regional aircraft based on web flight data," in *Proc. Int. Conf. Power Electron. Drives Energy Syst. (PEDES)*, 2018, pp. 1–6.

[25] Eurocontrol, "Aircraft performance database." [Online]. Available: contentzone.eurocontrol.int/aircraftperformance/

[26] A. Barzkar and M. Ghassemi, "Electric power systems in more and all electric aircraft: A review," *IEEE Access*, vol. 8, pp. 169 314–169 332, 2020.

[27] V. Gkoutzamanis, S. Tsentis, O. Valsamis Mylonas, A. Kalfas, K. Kyprianidis, P. Tsirikoglou, and M. Sielemann, "Thermal management system considerations for a hybrid-electric commuter aircraft," *J. Thermophys. Heat Transfer*, pp. 1–17, 03 2022.

[28] P. M. Sforza, "Direct calculation of zero-lift drag coefficients and (L/D) max in subsonic cruise," *J. Aircr.*, vol. 57, no. 6, pp. 1224–1228, 2020.

[29] "Rolling Resistance, *The Engineering ToolBox*," https://www.engineeringtoolbox.com/rolling-friction-resistance-d_1303.html.

[30] "Drag Coefficient, *The Engineering ToolBox*," https://www.engineeringtoolbox.com/drag-coefficient-d_627.html.

[31] D. Raymer, *Aircraft Design: A Conceptual Approach, Sixth Edition*, 09 2018.

[32] Siemens, "eAircraft: Disrupting the way you will fly!" last accessed 30 December 2023. [Online]. Available: https://www.ie-net.be/sites/default/files/Siemens%20eAircraft%20-%20Disrupting%20Aircraft%20Propulsion%20-%20OO%20JH%20THO%20-%2020180427.cleaned.pdf

[33] Rolls-Royce, "Powering Regional Air Mobility: Electric propulsion unit (EPU) for commuter aircraft applications," last accessed 30 December 2023. [Online]. Available: https://www.rolls-royce.com/~/media/Files/R/Rolls-Royce/documents/others/rolls-royce-regional-air-mobility.pdf

[34] Airbus, "Airbus' high-voltage battery technology prepares for EcoPulse flight test and beyond, 2022," https://www.airbus.com/en/newsroom/news/2022-03-airbus-high-voltage-battery-technology-prepares-for-ecopulse-flight-test.

[35] G. Valente, S. Sumsurooah, C. I. Hill, M. Rashed, G. Vakil, S. Bozhko, and C. Gerada, "Design methodology and parametric design study of the on-board electrical power system for hybrid electric aircraft propulsion," in *Proc. Int. Conf. Power Electron. Mach. Drives (PEMD)*, vol. 2020, 2020, pp. 448–454.

[36] J. M. Rheaume, M. Macdonald, and C. E. Lents, "Commercial hybrid electric aircraft thermal management system design, simulation, and operation improvements," in *Proc. AIAA/IEEE Electr. Aircr. Technol. Symp. (EATS)*, 2019, pp. 1–23.

[37] H. Kellermann, S. Fuhrmann, M. Shamiyeh, and M. Hornung, "Design of a battery cooling system for hybrid electric aircraft," *J. Propul. Power*, vol. 38, no. 5, pp. 736–751, 2022.

[38] P. M. Sforza, "Chapter 10 - propellers," in *Theory of Aerospace Propulsion (Second Edition)*, second edition ed., ser. Aerospace Engineering, P. M. Sforza, Ed. Butterworth-Heinemann, 2017, pp. 487–524.

[39] W. Lammen and J. Vankan, "Energy optimization of single aisle aircraft with hybrid electric propulsion," in *Proc. AIAA SciTech Forum*, 2020, p. 0505.

[40] J. C. Chin, E. D. Aretskin-Hariton, D. J. Ingraham, D. L. Hall, S. L. Schnulo, J. S. Gray, and E. S. Hendricks, "Battery evaluation profiles for X-57 and future urban electric aircraft," in *Proc. AIAA/IEEE Electr. Aircr. Technol. Symp.*, 2020, pp. 1–13.